2024

SEA LEVEL RISE DRIVEN GROUNDWATER INUNDATION: EFFECTS OF ISLAND HYDROGEOLOGY ON FRESHWATER LENS DYNAMICS

Lauren K. Mancewicz
Michigan Technological University, lkmancew@mtu.edu

SEA LEVEL RISE DRIVEN GROUNDWATER INUNDATION: EFFECTS OF ISLAND HYDROGEOLOGY ON FRESHWATER LENS DYNAMICS

By

Lauren K. Mancewicz

A DISSERTATION

Submitted in partial fulfillment of the requirements for the degree of

DOCTOR OF PHILOSOPHY

In Environmental Engineering

MICHIGAN TECHNOLOGICAL UNIVERSITY

2024

This dissertation has been approved in partial fulfillment of the requirements for the Degree of DOCTOR OF PHILOSOPHY in Environmental Engineering.

Department of Civil, Environmental, and Geospatial Engineering

Dissertation Co-Advisor:	*Alex Mayer*
Dissertation Co-Advisor:	*David Watkins*
Committee Member:	*John Gierke*
Committee Member:	*Jason Gulley*
Committee Member:	*Christian Langevin*
Committee Member:	*Jonathan Martin*
Department Chair:	*Brian Barkdoll*

Dedication

To my mom and dad. Thank you for always supporting me while I figure out my algebra homework.

Table of Contents

Author Contribution Statement

Chapter 2 of this dissertation, “ Improved method for simulating groundwater inundation using the MODFLOW 6 Lake Transport Package” has been published in Groundwater in September 2022. It is authored by Lauren Mancewicz, Alex Mayer, Christian Langevin and Jason Gulley.

Acknowledgements

I wish to express my sincere gratitude to my co-advisor, Dr. Alex Mayer, who has been an invaluable source of support and knowledge throughout my degree. His kindness, encouragement, and mentorship have greatly enriched and shaped my doctoral journey. I am also grateful to my co-advisor, Dr. Dave Watkins, whose willingness to offer assistance has been greatly appreciated. I would like to express my gratitude to committee member Dr. Chris Langevin. The knowledge and skills gained from his mentorship were indispensable to the completion of my research. Special thanks are due to committee members Dr. Jon Martin and Dr. Jason Gulley, whose technical expertise significantly contributed to this research. Their insights were instrumental in developing this work. Additionally, I extend my thanks to Dr. John Gierke, who was my advisor for an undergraduate research project several years ago, for his enduring impact on my academic endeavors. Collectively, the support and guidance from my advisors and committee members have been indispensable to the completion of this dissertation.

I am also sincerely grateful to G, who provided essential technical support throughout the completion of my research. Additionally, I would like to thank the CEGE Department, Graduate School, and SMART Program for their generous funding support.

I want to express my heartfelt gratitude to my partner, Taylor, whose unwavering love, patience, and dedication have been the anchor that kept the other aspects of my life afloat during the pursuit of my degree. I am profoundly grateful for his enduring support and understanding.

I am immensely thankful for the unwavering support of my parents. Their pride in my achievements serves as a constant source of motivation. Throughout my degree, they have always been there for me, offering consistent encouragement which I am deeply grateful for. I also extend my gratitude to my brother Joel and sister-in-law Kathryn, whose PhD starter kit has carried me through. I express my sincere appreciation to my grandparents for their invaluable words of wisdom and unwavering encouragement and to the rest of my extended family for rooting me on all this time. I also want to extend my heartfelt thanks to Nihar, Danielle, Mahta, Ellen, and Charlie. Their unwavering support, shared laughter, moral encouragement, and enthusiastic cheerleading have been vital components of my journey.

Abstract

Groundwater inundation due to sea level rise poses a threat to fresh groundwater availability in coastal areas, and small islands are particularly vulnerable. On an island, when sea level rises, the freshwater lens also rises due to the difference in density between the salt and fresh groundwater. As the water table rises above the land surface it forms a lake and the water is exposed to additional evaporative losses, reducing the amount of fresh water available. This work aims to improve our understanding of groundwater inundation due to sea level rise and the impact of different hydrogeologic settings and phenomena on lake salinity and the freshwater lens. We showcase using the Lake Transport package, a groundwater modeling tool for MODFLOW 6, to model groundwater inundation in a more physically accurate and computationally efficient way compared to past methods. We used these methods to investigate a common hydrogeologic setting where an upper low hydraulic conductivity layer is underlain by a high hydraulic conductivity layer in order to understand the impact of groundwater inundation of the layered system compared to a homogeneous one. Ultimately, the initial condition, regardless of other factors, was most significant in determining the impact of groundwater inundation on the freshwater lens. We also explored a particular phenomenon called density driven instability or fingering events (DF events), where a higher density fluid overlies and intrudes into a less density fluid below it. This can occur between a lake formed by groundwater inundation and the underlying aquifer. The onset of a DF event and the impacts of an event on the freshwater lens are a function of five factors: changes in land surface recharge, upconing, evapoconcentration, the upward movement of the freshwater lens from SLR, and connection/isolation between the lake and aquifer.

1 Chapter 1: Introduction

Groundwater inundation due to sea level rise poses a threat to freshwater resources in coastal areas, especially in an island setting where the fresh groundwater is limited to the freshwater lens. As sea level rises the freshwater lens also rises (Rotzoll and Fletcher 2013; Masterson et al. 2014; Habel et al. 2017; Gulley et al. 2016; Mancewicz et al. 2023). Where the water table intersects the land surface, surface water features may form, exposing what was once groundwater to additional evaporative losses and reducing the size of the freshwater lens(Gulley et al. 2016; Mancewicz et al. 2023).

Using a numerical model to explore the impact of groundwater inundation due to sea level rise is a method that has been employed in other works (Bjerklie et al. 2012; Rotzoll and Fletcher 2013; Masterson et al. 2014; Gulley et al. 2016; Habel et al. 2017), however, past methods either do not capture all of the physical processes associated with groundwater inundation or do so in a computationally inefficient way. There is a need to be able to represent the lake – groundwater interactions in a more physically accurate and computationally efficient way so that we can gain a better understanding of impact of groundwater inundation due to sea level rise on freshwater resources for islands.

One common hydrogeologic setting encounter on islands is the presence of a low hydraulic conductivity layer that overlies a high hydraulic conductivity that is several orders of magnitude greater than the upper layer (Ayers and Vacher 1986; Griggs and Peterson, n.d.; Oberdorfer, Hogan, and Buddemeier 1990; Cant and Weech 1986; Whitaker and Smart 2000). While these types of islands have been the subject of several studies related to the extent of the freshwater lens (Ketabchi et al. 2014; Dose et al. 2014; Vacher 1988; Terry and Chui 2012), there have been few that incorporate sea level rise (Ketabchi et al. 2014; Terry and Chui 2012) and none to our knowledge that incorporate the groundwater – surface water dynamics related to groundwater inundation due to sea level rise. Since a two-layer islands with an upper layer of low hydraulic conductivity overlaying a high hydraulic conductivity layer is a common hydrogeologic setting, it is important to study this conceptual model in particular to understand the potential impact of groundwater inundation on the freshwater lens.

One phenomenon that may occur in association with groundwater inundation is density driven fingering (DF) events. A DF event can occur when fluid of a greater density overlies fluid with a lower density. The difference in density creates an unstable condition where a plume, or finger, of the high density fluid flows down into the low density fluid. This situation may develop between a lake formed by groundwater inundation (the more dense fluid) and the underlying aquifer below the lake (the less dense fluid). The onset of DF events has been studied within the context of a hypersaline lake, including those on small islands (Juster et al. 1997), as well as other coastal environments (Greskowiak 2014; Wu et al. 2022; van Duijn, Pieters, and Raats 2019; Post and Houben 2017). However, groundwater inundation due to sea level rise has not yet been considered as a setting for which DF events may occur. These events have the potential to further salinize the freshwater lens and require specific consideration.

The gaps in our understanding of groundwater inundation and the impact on the freshwater lens identified above will be addressed as follows. Chapter 1 contains this introduction to the remainder of the dissertation. Chapter 2 is titled “Improved method for simulating groundwater inundation using the MODFLOW 6 Lake Transport Package”. This chapter has been published in Groundwater (Mancewicz et al. 2023) and addresses improvements in how groundwater inundation due to sea level rise can modeled using a variable density groundwater flow and transport numerical modeling program. Chapter 3 is titled “Modeling the impacts of groundwater inundation on the freshwater lens and lake salinity for a multilayer aquifer” and addresses the impact of groundwater inundation on the specific setting of a two-layer island described above. Chapter 4 is titled “Density driven instabilities due to groundwater inundation from sea level rise may threaten island freshwater lens”. This chapter explores the impact of DF events on the freshwater lens and lake salinity. The results of Ch 2-4 have been synthesized in Chapter 5 Conclusions. Overall, this dissertation seeks to improve our understanding of groundwater inundation due to sea level rise and the threat to the freshwater lens for small islands.

2 Chapter 2: Improved method for simulating groundwater inundation using the MODFLOW 6 Lake Transport Package

2.1 Introduction

Groundwater inundation due to sea level rise and the effects on freshwater resources has been the focus of recent work (Bjerklie et al. 2012; Rotzoll and Fletcher 2013; Masterson et al. 2014; Gulley et al. 2016; Habel et al. 2017), yet a more complete understanding of groundwater inundation has been limited. Groundwater inundation occurs when the groundwater table rises above land surface causing flooding. The emerging significance of groundwater inundation and its effects on freshwater provides motivation for the development of new modeling tools to address this phenomenon and its effects on the freshwater lens. MODFLOW 6, the most recent version of MODFLOW, is a widely used numerical groundwater modeling program maintained by the U.S. Geological Survey (Hughes, Langevin, and Banta 2017; C.D. Langevin et al. 2022). This work aims to demonstrate the functionality and advantages of using the variable density capabilities in MODFLOW 6 (Langevin et al. 2020) with the recently created Groundwater Transport Model (Langevin et al. 2022). The Groundwater Transport Model includes the Lake Transport Package, which calculates changes in solute concentration within individual lakes based on solute budget calculations. These new capabilities are applied to simulate groundwater inundation on an island setting.

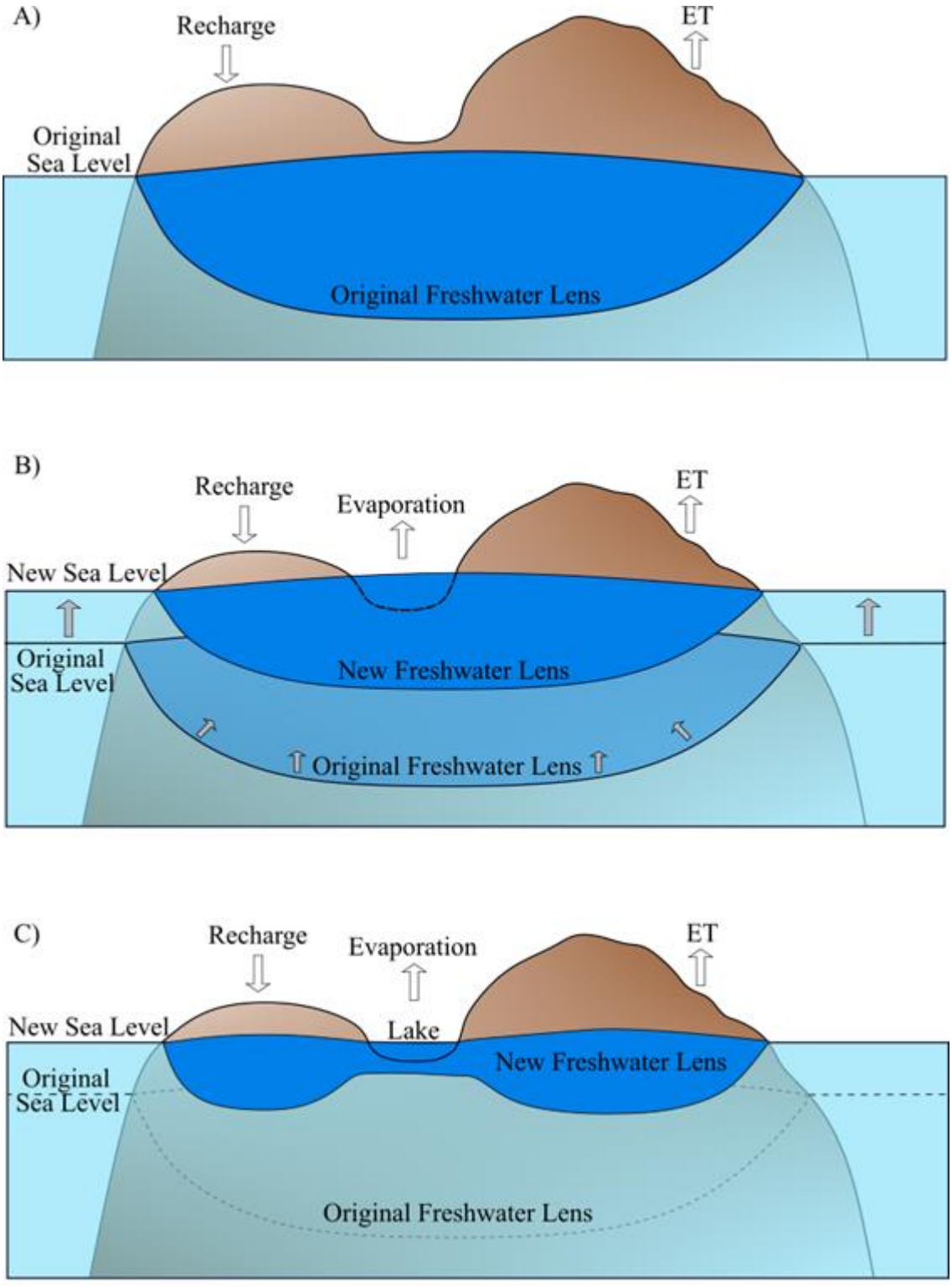

Figure 1: Process of groundwater inundation due to sea level rise for an island, where ET is evapotranspiration. (A) shows the original freshwater lens and sea level prior to sea level rise. As the sea level rises, the freshwater lens also rises, flooding low lying areas

(B). The newly formed lake exposes what was once fresh groundwater to evaporation, increasing freshwater lens losses and decreasing the freshwater lens volume (C).

In a homogeneous island aquifer, fresh groundwater occurs in a characteristic convex shape due to the density differences between fresh and salt water (see Figure 1A). This accumulation of fresh groundwater is known as the freshwater lens. The Ghyben-Herzberg equation (Ghyben 1889; Herzberg 1901) relates the depth of the freshwater lens below sea level (z) to the elevation of the water table above sea level (h) at equilibrium:

(1) $z = \alpha h$

where α is a density ratio defined as:

(2) $\alpha = \frac{\rho_f}{\rho_s - \rho_f}$

where ρ_f is the density of fresh groundwater and ρ_s is the density of saline groundwater. For typical densities of fresh and saline water of 1000 kg/m3 and 1025 kg/m^3, respectively, the depth of the freshwater lens below sea level is 40 times the height of the water table above sea level. Additionally, the hydrogeologic characteristics of the island-aquifer system, such as the hydraulic conductivity distribution, island size and topography, and net recharge rates influence the water table and extent of the freshwater lens.

Sea level rise and reductions in aquifer recharge, from climate change can negatively affect the freshwater lens, reducing the amount of fresh groundwater available for water supplies. As sea level rises, coastal areas can become inundated, decreasing island widths and shortening lateral groundwater flow path lengths, which in turn decrease the water table elevation relative to sea level (Gulley et al. 2016). According to the Ghyben-Herzberg ratio, the corresponding decrease in the depth to the base of the freshwater lens is 40 times the change in water table height. Thus, even a small change in the water table elevation can have a significant effect in the thickness of the freshwater lens. In addition to raising sea level, climate change may alter precipitation patterns and evapotranspiration rates, resulting in a loss of net recharge and further decreasing the freshwater lens size.

Groundwater inundation is an additional mechanism for freshwater lens depletion (see Figure 1). As sea level rises, the freshwater lens moves upwards, potentially flooding low-lying areas and expanding existing lakes and wetlands, or even creating new surface water features. For the groundwater lying below land surfaces, the effective recharge rate (precipitation rate minus evapotranspiration rate) is typically positive. However, if the groundwater is hydraulically connected to surface water, it is exposed to a negative effective recharge if the lake evaporation rate exceeds the precipitation rate. In this case, the surface water body essentially acts as a pump depleting the fresh groundwater lens (Gulley et al. 2016).

In recent work, Gulley et al. (2016) simulated groundwater inundation in a hypothetical island under steady state conditions with SEAWAT, a commonly used variable-density coupled groundwater flow and transport program (Guo and Langevin 2002; Christian D. Langevin et al. 2008). Because SEAWAT lacks the ability to model lakes directly, Gulley et al. (2016) represented a lake as a series of cells at the top of the aquifer with high hydraulic conductivity (K) relative to the surrounding aquifer and 100% porosity. The intention of this approach was to allow flow and solute exchange between the lake cells and the aquifer cells, while generating constant heads in the lake cells such flow was insignificant within the lake cells. To model the effect of sea level rise and the associated groundwater inundation and lake expansion using this "high-K" approach, the user must determine the lateral extent of the lake cells for each combination of sea level rise rate, lake bathymetry, and elapsed time. The lateral extent of the lake cells is computed external to the SEAWAT model and the input files for the aquifer properties and boundary conditions must be adjusted accordingly.

While application of the "high-K" approach has provided insights to the relative effect of sea level rise and groundwater inundation on island freshwater lenses, this approach has some limitations. First, the approach method requires the user to perform external calculations and manually update boundary conditions and aquifer property input files, as well as complete additional post processing to obtain flow and transport budgets for the lake (Hunt et al. 2003). Additionally, numerical conditions in the lake cells can potentially lead to longer run times and result in unrealistic spatial gradients in hydraulic head and salinity (Merritt and Konikow 2000; Mulligan, Langevin, and Post 2011). These gradients can affect the flux of water and solute into and out of the lake thereby affecting the lake salinity and the surrounding groundwater. Furthermore, the high-K approach can lead to numerical instability due to the several orders of magnitude difference in hydraulic conductivity between lake and aquifer cells that are adjacent to one another (Merritt and Konikow 2000; Mulligan, Langevin, and Post 2011).

The original MODFLOW Lake Package calculates lake stage and volume from the lake water balance, which includes Darcy-flux-based exchange between the lake and the aquifer (Cheng and Anderson 1993). Later versions included improved solution methods and incorporated additional lake characteristics such as irregular bathymetry that allows for lakes to coalesce depending on the stage and for a lake to dry and rewet (Council 1997; Merritt and Konikow 2000; Christian D. Langevin et al. 2017). Additionally, the Lake3 Package has the ability to simulate solute exchange between a lake and the aquifer when used with MOC3D, a solute transport model compatible with previous versions of MODFLOW (Konikow, Goode, and Hornberger 1996; Merritt and Konikow 2000).

The ability to simulate solute transport between a lake and the aquifer, as done with the Lake3 Package, is critical for being able to represent groundwater inundation. In this paper, we extend previous work on MODFLOW lake packages by implementing lake transport processes into the MODFLOW 6 framework. This allows us to take advantage of recent MODFLOW advances, not available in previous MODFLOW versions, that are beneficial for representing groundwater inundation. For example, the MODFLOW 6 Lake Package supports the Newton formulation, which improves numerical convergence

for layer wetting and drying conditions commonly encountered in island settings due to sea level fluctuations. Additionally, while not used in our study, MODFLOW 6 supports unstructured grids whose flexibility is beneficial for efficiently discretizing irregularly shaped islands. Also, MODFLOW 6 supports multi-species simulations where different species (e.g., nutrients, tracers, heat) can be incorporated in an equation of state for density, affecting flow between the lake and aquifer. Also, when using the Buoyancy Package in MODFLOW 6 along with the Lake Transport Package, both solute transport between the lake and aquifer and variable density flow can be accounted for (Langevin et al. 2022). By combining the Lake Package and the Lake Transport Package, MODFLOW 6 provides a way to model groundwater inundation in a way that is more physically accurate while overcoming the limitations encountered with using SEAWAT and the high-K approach.

The Lake Package is a head-dependent flux boundary package within the Groundwater Flow Model that calculates water fluxes between a lake and the aquifer (Langevin et al. 2017). The stage of the lake is calculated according to changes in the flow budget for the lake. As the lake stage changes, the lake surface area is recalculated according to bathymetry specified by the user. Consequently, lake flux boundary conditions, such as precipitation and evaporation, are automatically adjusted to reflect the change in lake surface area. As the lake expands, cells with aquifer boundary conditions are reassigned to lake conditions. As the lake contracts, former lake cells are converted to aquifer cells with aquifer boundary conditions (Langevin et al. 2017). These flow and stage changes are recalculated for each Picard iteration loop; the solution is not considered converged until these changes are less than user-specified tolerances. Using the Lake Package in MODFLOW 6 to represent a lake, as opposed to the high-K approach with SEAWAT, eliminates the need for external calculations of lake stage and extent of the lake. Additionally, the Lake Package does not require boundary conditions and aquifer properties to be manually updated with external calculations as they do with the high-K approach. These features of the Lake Package allow for sea level rise-lake expansion simulations to be run straightforwardly with a single simulation.

2.2 Methods

2.2.1 Representing Groundwater Inundation using the Lake and Lake Transport Packages

The recently developed MODFLOW 6 Lake Transport Package is part of the Groundwater Transport Model and has been successfully tested with existing constant density lake transport examples (Langevin et al. 2022). The Lake Transport Package accommodates transport and variable density flow into and out of the lake. The concentration of the solute in the lake is calculated with the following mass balance, assuming instantaneous and uniform mixing within the lake:

$$C^i = \frac{C^{i-1}V^{i-1} + \sum_j Q_j^i C_j^i \Delta t}{V^i}$$

(3)

where C is the solute concentration in the lake at the current (i) or previous (i-1) time step, j is the lake cell index at time i, V is the volume of the lake, Q_j is the flux into or out of the lake cells associated with the aquifer, and C_j is the solute concentration in the lake cells associated with the aquifer for flux out of the lake or the solute concentration in the aquifer cells associated with the lake for flux into the lake, and Δt is the duration of the time step. Additionally, the Lake Package for flow and the Lake Transport Package are capable of accommodating the effects of density variations by implementing a variable density form of Darcy's Law based on hydraulic head (Langevin et al. 2020). The code for the Lake Transport Package is available as part of the Groundwater Transport Model for MODFLOW 6 (Langevin et al. 2021).

2.2.2 Example Island with a Lake and Sea Level Rise

To demonstrate the functionality of the Lake and Lake Transport Packages, within the context of sea level rise and groundwater inundation on an island, we created a two dimensional (2D) variable density flow and transport model for a hypothetical 1000 m wide strip island. MODFLOW 6 version 6.2.2 (Langevin et al. 2021) was used with FloPy (Bakker et al. 2021), a Python package used to create the MODFLOW input files, run simulations, and post process results. The hydrogeologic properties and conceptual model for these simulations were based on the carbonate platform islands of the Bahamas, similar to Gulley et al. (2016) (Table 1). Due to the symmetry of the hypothetical island, only half of the island was modeled, resulting in a 500 m wide domain. The top of the domain was set to 4.4 m above sea level (ASL) and the bottom to -40.6 m ASL with cell dimensions of 2 m in the lateral direction by 1 m in the vertical direction. We defined freshwater as having a solute concentration equal to or less than 1.0 g/L and the freshwater lens size was defined as the total number of freshwater cells at a given timestep divided by the initial number of freshwater cells for that simulation.

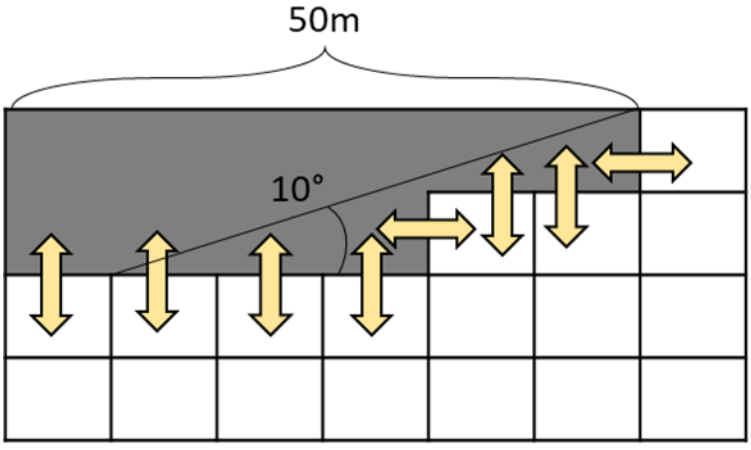

Figure 2: General geometry of the lake showing the designation of the lake connection cells. The size of the cells are not to scale, but instead show the relative setup of the lake for the Lake Package. The lake is indicated in gray and consists of inactive cells.

Connections between the lake and aquifer can be vertical, horizontal, or both as indicated by the arrows.

The surface topography had an area of lower elevation located at the center of the island. As sea level rose in transient simulations, this depression became inundated with groundwater, forming a half lake. The depression was 50 m wide along the bottom, which was set at an elevation of 0.4 m ASL. The lake bathymetry had a constant slope of 10 degrees from the bottom edge of the depression to the top of the model domain (Figure 2). Vertical and horizontal lake connection cells were specified as shown in Figure 2. Aquifer cells adjacent to the lake were assigned relatively high values for the storage properties (1.0 m-1 for specific storage) applied when the hydraulic head is above the cell top. These large storage values improved convergence of the flow solution as cells transitioned from partially saturated to fully saturated. We specified evapotranspiration (ET) and land surface precipitation for the uppermost active cells in the aquifer with a maximum ET rate equal to recharge (0.00055 m/d). A no-flow boundary condition was used along the bottom and left edge of the domain. The coastal boundary was represented with a vertical face along the right side of the model domain using the general head boundary (GHB) package with salinity equal to sea water (35 g/L). The hydraulic head was set equal to sea level and the conductance was set to 20 m2/d. To generate initial conditions, we ran a spin up simulation with sea level (GHB head) set to 0 m and all other boundary conditions as specified above. We ran the spin up simulation until the consecutive change in the average salinity was less than 10-6 g/L and the maximum change in salinity for a single cell was less than 10-10 g/L. A timestep of 5 days with one stress period was used for the spin up simulation and the solution resulted in the lake being dry with the water table below the bottom of the lake. Additional hydrologic parameters are shown in Table 1.

Table 1: Values used for aquifer properties and model domain setup.

Property	Value
Cell dimensions (m, in the x, y, z directions)	2 x 1 x 1
Top elevation (m)	4.4
Bottom elevation (m)	-40.6
Domain width (m)	500
Vertical hydraulic conductivity (m/d)	20
Horizontal hydraulic conductivity (m/d)	20
Specific storage (m^{-1})	0.008, 1.0 for lake connection cells
Porosity	0.30
Longitudinal dispersivity (m)	1.0
Transverse dispersivity (m)	0.1
Aquifer recharge (m/d)	0.00055
Maximum evapotranspiration (m/d)	0.00055
ET cutoff depth relative to surface elevation (m)	2.0
Lake rainfall (m/d)	0.00055
Lake evaporation (m/d)	Varied; 0.0019, 0.0011, 0.0006
SURFDEP[1] (m)	1.0

Lakebed leakance (d^{-1})	4.0

[1] SURFDEP is a smoothing parameter used to represent depressions in the bottom surface of a lake that can also aid in convergence

We ran eight transient simulations with varying sea level rise rates and effective recharge rates for a total duration of 200 years with a time step of 5 days, using the spin up results as the initial condition for each simulation (Table 2). We used a high and a low sea level rise rate of 0.01m/yr (1 m/100 yr) and 0.02 m/yr (2 m/100 yr), respectively. Sea level rise was represented by changing the hydraulic head in the general head boundary condition within MODFLOW 6. We conducted sea level rise simulations with and without a lake. For the sea level simulations with a lake, the lake rainfall and evaporation rates were $5.5x10^{-4}$ m/d and $6.6x10^{-4}$ m/d, respectively, which are typical for the central Bahamian islands (Gulley et al. 2016) and give a slight net negative water loss for the lake. We conducted two more sets of sea level rise simulations with a lake with higher evaporation rates of $1.1x10^{-3}$ m/d and $1.75x10^{-3}$ m/d to simulate hypersaline lake solute concentrations and the greater effects from upconing of the freshwater lens underneath the lake. The flow and solute mass balance errors for all simulations were less than 0.1% and 0.01% respectively.

2.3 Results

For the simulations with a lake, as the freshwater lens rose in parallel with sea level rise, groundwater inundated the area of low topography, increasing the lake stage (Figure 3). The lake stage increased more quickly and groundwater inundation is greater with the lower evaporation rates and high sea level rise scenario. Lower evaporation rates resulted in smaller losses from the lake water budget compared to higher evaporation rates and a greater lake stage. With higher evaporation rates, more water was lost from the lake, which reduced the lake stage. As sea level rose, so did the freshwater lens and the water table. Thus, higher sea level rise rates also increased the lake stage more quickly because the freshwater lens and water table were also rising at a quicker rate. Additionally, the rate of change in lake stage relates to the rate of change in lake salinity (Figure 4). As the lake stage increased, the lake expanded increasing the lake surface area. As the surface area increased, the amount of water lost from evaporation also increased, raising the lake salinity. Directly increasing the evaporation rate similarly increases the lake salinity.

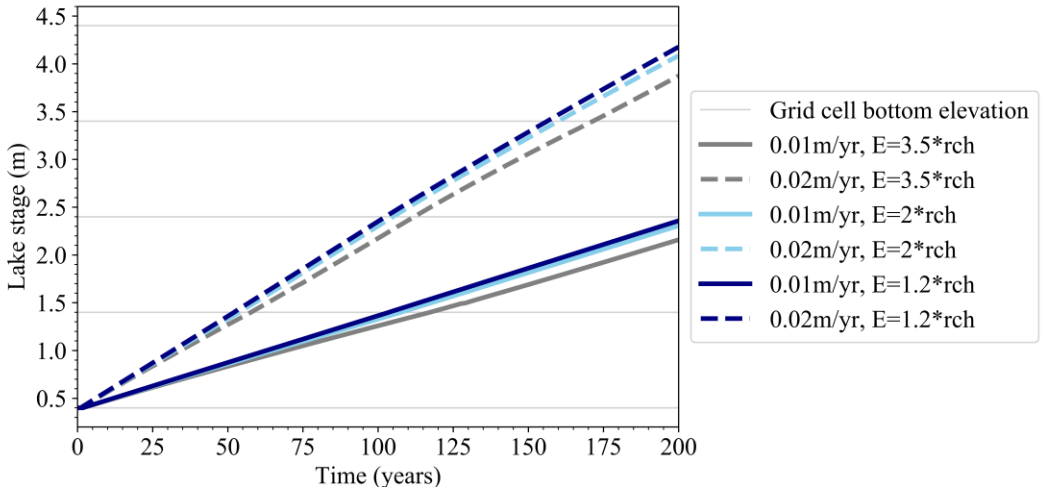

Figure 3: Change in lake stage over time for each simulation with a lake where E is the evaporation rate and rch is the recharge rate. At the beginning of each simulation, the water table starts off below the lake bottom and the lake is dry, briefly resulting in a constant lake stage at 0.4 m until the water table inundates the area of lower topography forming the lake. The elevation of the bottom of each grid cell connected to the lake is shown in gray. Once the lake stage is greater than the bottom elevation, a new row of connection cells are "turned on." The stage increases more rapidly for the high sea level rise simulations and for those with lower lake evaporation rates.

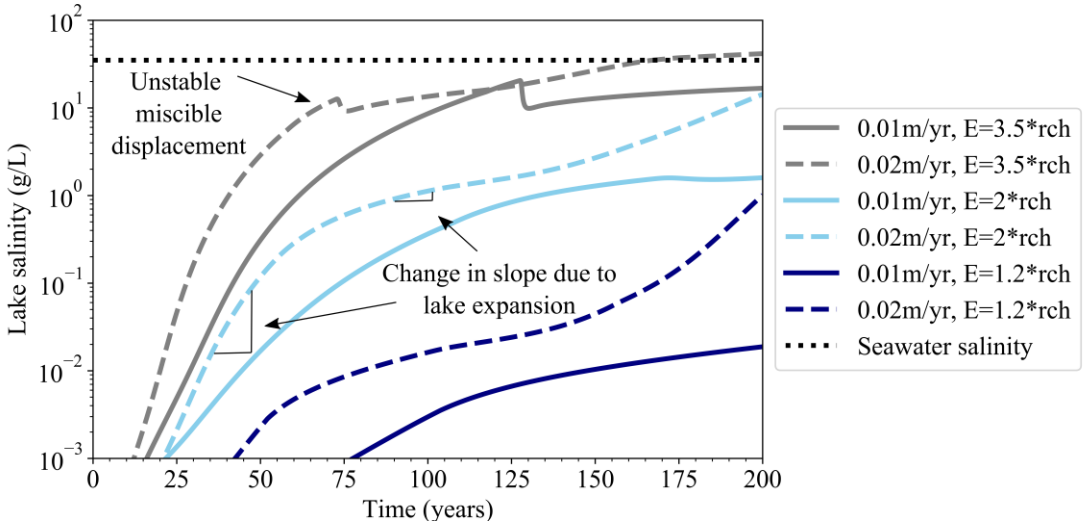

Figure 4: Change in the lake concentration as calculated by the Lake Transport Package where E is the evaporation rate and rch is the recharge rate. The concentration of seawater is also shown for reference (35 g/L). Greater evaporation and sea level rise rates result in higher concentrations. The results were truncated at 10-3 g/L. The annotations

highlight an event of miscible displacement that affected the lake salinity and the response of lake salinity to the initial lake expansion.

In the case of extreme lake evaporation (3.5 x recharge) and a rate of 0.02 m/yr for sea level rise, unstable miscible displacement appears to occur (Figure 5). Unstable miscible displacement similarly occurred in the extreme lake evaporation with a low sea level rise rate simulation at year 128 and the high lake evaporation with a low and high sea level rise rate simulation at year 172 and 120 respectively. For the extreme evaporation rate scenario, several other timesteps had unstable miscible displacement that occurred to a much lesser extent and did not appear to substantially affect the lake salinity.

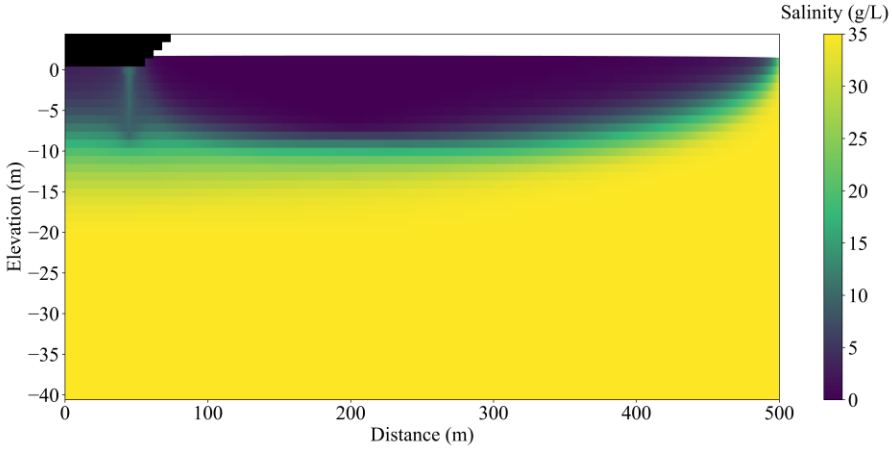

Figure 5: Concentration cross section showing unstable miscible displacement underneath the lake at 0m elevation and 45m from the left boundary for the extreme evaporation with high sea level rise scenario at time equal to 73 years. Elevation is shown on the y-axis and distance is shown along the bottom. The color bar shows the lake concentration in g/L with dark blue representing freshwater and yellow representing salt water. The area in black are cells that have been inactivated representing the possible extent of the lake. The white line shows the mass flow rate (g/d) from the lake to the aquifer connection cells where positive values indicate the movement of mass into the lake, and negative values represent mass moving out of the lake into the aquifer.

The loss of surface freshwater from lake evaporation not only affected the lake salinity, but also the extent of the fresh groundwater lens. Depending on the lake evaporation rate, the presence of a lake increased the loss of freshwater from the freshwater lens over the 200-year simulation period by 6.1 to 36.2% and 6.54 to 14.5% relative to an island without a lake, with sea level rise rates of 0.01m/yr and 0.02 m/yr, respectively. The higher lake evaporation rates resulted in greater freshwater lens depletion (Figure 6, Table 2). The freshwater lens curves in Figure 6 are not particularly smooth due to the discrete nature of counting individual model cells that meet the freshwater criteria.

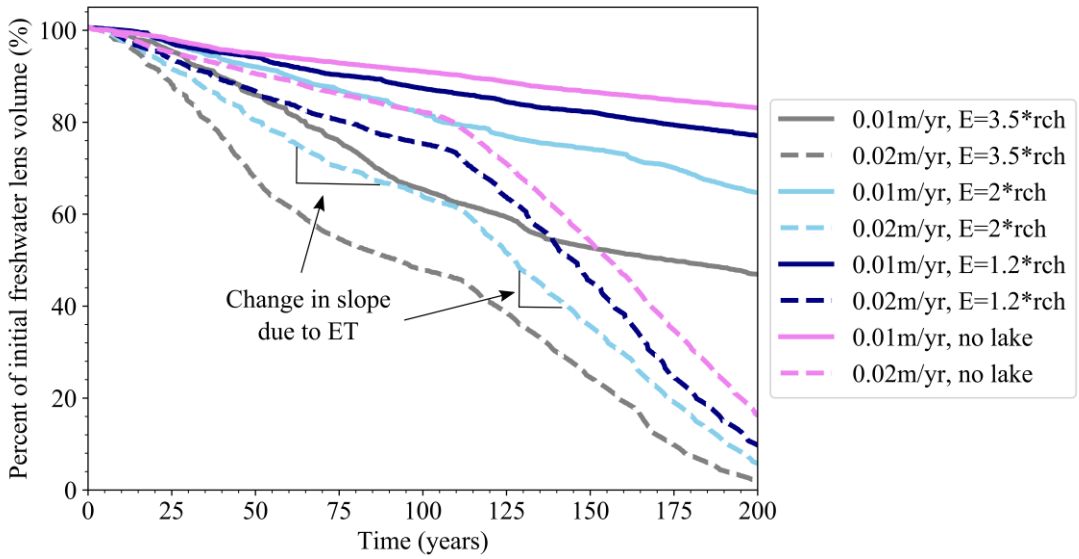

Figure 6: Freshwater lens volume as a percentage of the initial freshwater lens volume where E is the evaporation rate and rch is the recharge rate. The annotations highlight an event of miscible displacement and the response of the freshwater lens depletion rate in response to evapotranspiration (ET).

Table 2: Summary description of the simulations and the results for each simulation at the final timestep

Description (lake evaporation / sea level rise rate)	Sea level rise rate (m/yr)	Lake evaporation rate relative to recharge	Lake evaporation (m/d)	Final freshwater lens volume (% of initial lens volume)	Final lake concentration (g/L)
Extreme / low	0.01	3.5 x recharge	0.0019	46.9	16.8
Extreme / high	0.02	3.5 x recharge	0.0019	1.79	41.6
High / low	0.01	2 x recharge	0.0011	64.6	1.60
High / high	0.02	2 x recharge	0.0011	5.78	14.3
Low / low	0.01	1.2 x recharge	0.0006	77.0	0.02
Low / high	0.02	1.2 x recharge	0.0006	9.76	1.01
No lake / low	0.01	--	--	83.1	--
No lake / high	0.02	--	--	16.3	--

Distinct changes also were evident in the rate of freshwater lens depletion for the simulations with the higher sea level rise rate compared to the lower sea level rise rate. In the higher sea level rise rate simulations, the water table rose closer to the surface increasing ET, the rate of which varies linearly from 0 m/d at the cutoff depth of 2 m to 0.00055 m/d at the surface. As the rate of ET increased, freshwater was more quickly lost from the freshwater lens resulting in the steeper slopes of the curve observed in

Figure 6 for the simulations with a sea level rise rate of 0.02 m/yr. Additionally, this change in the slope shown in Figure 6 around 105 years occurs ~5 years earlier for the simulation without a lake and later for the simulation with a lake. The difference in timing resulted from freshwater being lost to the lake due to evaporation, which slows the rise in the water table. Therefore, it takes slightly longer for the water table to reach the cutoff depth for ET. Variations in the slope of the lens depletion curves also show the effects of unstable miscible displacement. In simulations that exhibit unstable miscible displacement the depletion of the lens briefly accelerated as the finger of more saline water moves from the lake into the aquifer, as can be seen from years 165 – 175 for high evaporation with the low sea level rise simulation.

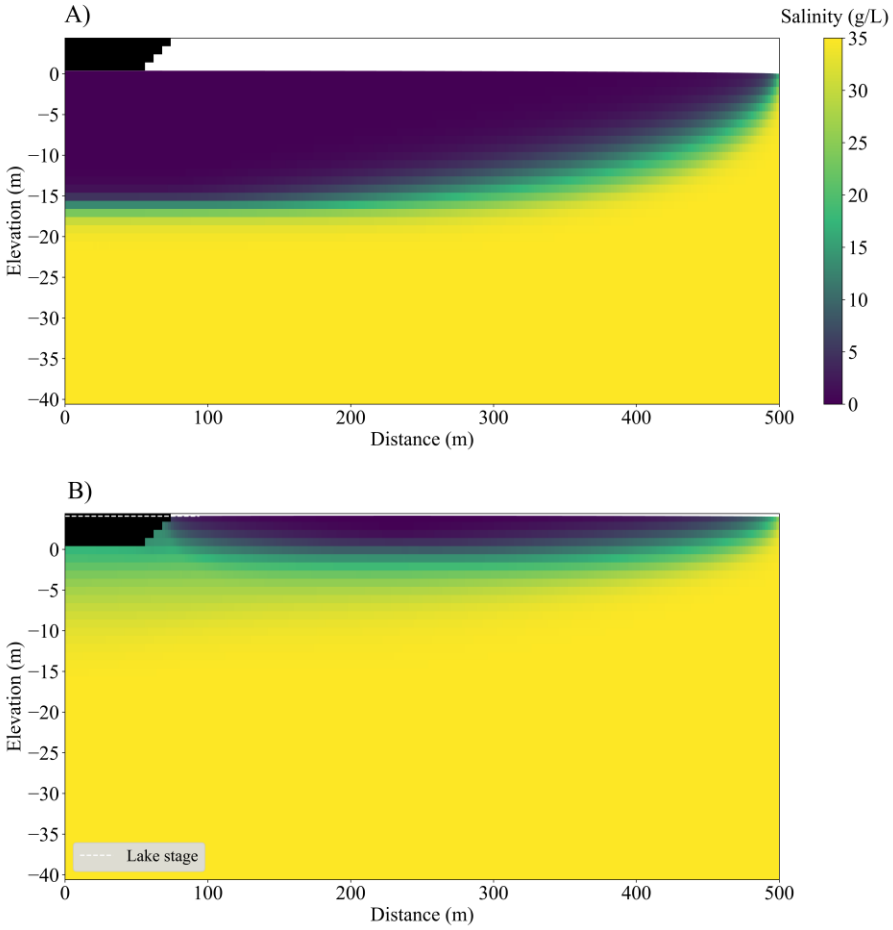

Figure 7: Concentration cross section for the high lake evaporation (2 x recharge) with a high sea level rise rate (0.02 m/yr). The initial conditions are presented in A where the water table is just below the bottom of the lake and the lake is dry. B shows the same scenario after 200 years of sea level rise with the lake at a stage of 4.1 m above sea level. As the sea level rises and the lake becomes inundated, fresh groundwater is lost to the lake through evaporation resulting in a decrease in the volume of the freshwater lens.

The depletion of the freshwater lens is illustrated in Figure 7, which shows the difference in the salinity cross-section between the initial conditions and the final timestep for the sea level rise simulation for an island with a lake under the high sea level rise, high lake evaporation scenario. In this scenario, the final freshwater lens was only 5.78% of initial lens volume. Additionally, the freshwater lens no longer extended underneath the lake and in the case of a full island, as opposed to the half island modeled in the domain, the freshwater lens would be fractionated.

2.4 Discussion

In regard to unstable miscible displacement, as freshwater from the lake was lost due to excessive evaporation, salt accumulated within the lake causing instability between the two fluids resulting from the density differences between the lake and the aquifer. This results in "fingering" of denser lake water plumes protruding into the less dense groundwater. Predicting the onset of and modeling unstable miscible displacement is a difficult task, but minimizing general numerical errors and increasing dispersion (if appropriate) may be helpful when fingering occurs (Schincariol, Schwartz, and Mendoza 1994; Diersch and Kolditz 2002; Greskowiak 2014). In this simulation, the lake salinity dropped at approximately 70 years before continuing to increase (Figure 4). At this point, unstable miscible displacement occurred along the right side of the lake as a finger of higher density lake water with a salinity of approximately 10 g/L moved downward underneath the lake before being diluted by the aquifer (Figure 5). Unstable miscible displacement is known to occur even for small differences in density and at low concentrations less than 10 g/L (Schincariol, Schwartz, and Mendoza 1994; Habtemichael, Kiflemariam, and Fuentes 2014). At the same time, the flow on the right side of the lake changed direction from into the lake to into the aquifer. Mass was lost from the lake into the aquifer connection cells at that location due to unstable miscible displacement that occurred below the lake, as shown in Figure 5, reducing the lake salinity and supporting this interpretation. Eventually, the salinity in the lake began to increase again due to the net loss of freshwater from evaporation.

It is also of note that for the high sea level rise simulations, the rate of change in lake salinity is low in the middle of the simulation and relatively high in the beginning and end (Figure 4). This result is related to the geometry of the lake and the hydraulic connection between the lake and the aquifer. At approximately 60 years, the lake expanded, inundating the next layer of grid cells above the original extent of the lake. This mechanism converted the next row of connection grid cells from aquifer cells to lake cells within the Lake Package. The new hydraulic connections between the lake and aquifer allowed fresh groundwater to flow into the lake and temporarily dilute the lake salinity. Later towards the end of the simulation at approximately 150 years, not only did the lake salinity increasing due to evaporation, but as the freshwater lens was depleted, the solute concentration of inflowing groundwater also increased leading to a greater increase in lake salinity.

Overall, these simulations demonstrated the ability of the Lake Transport Package to calculate the transient lake solute concentration due to groundwater inundation from sea

level rise under a variety of sea level rise and lake evaporation rates, showing the effect of groundwater induction on freshwater lens depletion. The lake salinity and freshwater lens depletion varied among the scenarios in an intuitive manner. For a given lake evaporation rate, the final lake salinity was greater for the higher sea level rise rate and for a given sea level rise rate, the final lake salinity increased with increasing lake evaporation. This work also demonstrated the ability of the Lake Transport Package to calculate hypersaline lake solute concentrations, as was observed in the extreme lake evaporation / high sea level rise scenario where the final salinity in the lake was 41.6 g/L.

It is important to note, however, that the Lake Transport Package assumes instantaneous and uniform mixing throughout the lake and does not account for lake dynamics, such as stratification. Additionally, these simulations were run for a homogeneous subsurface and more robust testing that includes heterogeneity in the properties that govern the lake-aquifer interaction, such as lakebed leakance, would be beneficial. Future work could involve using the Lake Transport Package to investigate groundwater inundation under several different hydrogeologic settings and lake types found on carbonate platform islands. Although this work focused on the application of the Lake Transport Package to groundwater inundation on an island, the Lake Transport Package can also simulate other situations where variable density flow and transport between a lake, or similar surface water feature, and an aquifer is a significant process. This could include simulating mine waste pits, waste lagoons, or coastal wetlands.

2.5 Conclusion

Utilizing the Lake Transport Package can provide a better insight to the effect of groundwater inundation on freshwater resources for small islands. The results from simulations representing groundwater inundation provide a qualitative assessment on the behavior of the Lake Transport Package and demonstrate the ability of this MODFLOW 6 package to calculate the lake solute concentration for transient simulations. Compared to past methods of representing groundwater inundation, the Lake Transport Package provides a method to represent the process in an improved way that is more physically accurate, computationally efficient, and allows for the calculations of lake solute concentration.

2.6 Acknowledgements

The authors would like to thank Kalle Jahn of the U.S. Geological Survey and two anonymous reviewers for their constructive comments on the paper. This material is based upon work that is supported by the National Science Foundation (award number 1743370). Any use of trade, firm, or product names is for descriptive purposes only and does not imply endorsement by the U.S. Government.

3 Chapter 3: Modeling the impacts of groundwater inundation on the freshwater lens and lake salinity for a multilayer aquifer

3.1 Introduction

Groundwater inundation due to sea level rise can limit the extent of the freshwater lens and availability of freshwater resources (Bjerklie et al. 2012; Rotzoll and Fletcher 2013; Masterson et al. 2014; Gulley et al. 2016; Habel et al. 2017). As sea level rises, the freshwater lens also rises and in low lying areas the water table may rise above the land surface creating new or expanding existing lakes and wetlands. This surface water is now subject to additional evaporative fluxes and leads to an increased loss of freshwater (Rotzoll and Fletcher 2013; Gulley et al. 2016; Mancewicz et al. 2023). There is growing interest and concern in regard to the impact of groundwater inundation on fresh groundwater (Yu et al. 2022; Chambers et al. 2023; Alsaffar, Hamed, and Majeed 2023). One common feature among small carbonate islands is the presence of two distinct geologic layers that vary in hydraulic conductivity by several orders of magnitude and constrain the extent of the freshwater lens. Representing a heterogeneous two layered aquifer as homogeneous in modeling simulations makes a difference in the size and shape of the freshwater lens and is a significant oversimplification (Ketabchi et al. 2014). It is thus important to understand how groundwater inundation due to sea level rise may impact layered freshwater aquifers on small islands, as well as the corresponding effect on lake-aquifer interactions under varying hydrogeologic settings.

The general shape of a freshwater lens for a homogeneous aquifer of an island under hydrostatic conditions can be described by the Ghyben-Herzberg principle. The Ghyben-Herzberg principle relates the depth of the freshwater lens at a point to the height of the water table above sea level:

(1) $z=\alpha h$

where α is a density ratio defined as:

(2) $\alpha = \frac{\rho_f}{(\rho_s - \rho_f)}$

where ρf is the density of fresh groundwater and ρs is the density of saline groundwater.

The extent of the freshwater lens for an island with two layers of varying hydraulic conductivity deviates from the Ghyben-Herzberg principle and has been the subject of a number of modeling studies. This geologic configuration has the effect of truncating the freshwater lens near the boundary between the two layers, deviating from the idealized Ghyben-Herzberg freshwater lens shape. When streamlines cross an interface between high and low hydraulic conductivity units, they are refracted (Freeze and Cherry 1979). The refraction of streamlines across the boundary between the two layers is followed by a loss of pressure through the layer with the lower hydraulic conductivity. The pressure,

and consequently the downward force, at the interface is lower compared to the homogeneous Ghyben-Herzberg case, causing the base of the lens to draw upward and appear truncated (Ritzi et al. 2001).

These small islands with two distinct hydraulic conductivity layers exist in many parts of the world including several atolls in the Pacific and the Bahamas in the Caribbean (Ayers and Vacher 1986; Griggs and Peterson, n.d.; Oberdorfer, Hogan, and Buddemeier 1990; Cant and Weech 1986; F. F. Whitaker and Smart 2000; Fiona F. Whitaker and Smart 1997). Hydraulic properties on atoll islands vary vertically with a Holocene aquifer of low hydraulic conductivity overlying a Pleistocene limestone (Ayers and Vacher 1986). The contact between the two geologic units is known as the Thurber Discontinuity and ranges from a depth of 15 – 25m below the surface (Bailey, Jenson, and Olsen 2009). The upper younger Holocene layer is made of unconsolidated sediments with a hydraulic conductivity on the order of 10^1 m/d (Griggs and Peterson, 1993; Oberdorfer, Hogan, and Buddemeier 1990) The layer below the Thurber Discontinuity is composed of limestone that has undergone extensive diagenetic alteration, resulting in a hydraulic conductivity on the order of 10^3 m/d (Griggs and Peterson, 1993; Oberdorfer, Hogan, and Buddemeier 1990). The freshwater lens is truncated at the Thurber Discontinuity, making this contact between geologic layers a controlling feature in determine the shape and extent of the freshwater lens on atoll islands (Bailey, Jenson, and Olsen 2009).

The small carbonate islands of the Bahamas also typically consist of two main geologic units; an upper Pleistocene layer know as the Lucayan Limestone formation and a deeper, older pre-Lucayan layer. The Lucayan Formation extends to a depth of 21 – 43 m below sea level and has an average hydraulic conductivity of on the order of 10^1 m/d (Whitaker and Smart 2000). The local thickness of the Lucayan limestone is a function of regional folding (Pierson, 1982). The Pre-Lucayan Formation has undergone longer period of limestone alteration and consequently has a hydraulic conductivity up to three orders of magnitude greater than the Lucayan Limestone (Cant and Weech, 1986). Vacher and Wallis (1992) categorized this configuration of geology and resulting freshwater lens shape as the "Bahamas-type island." One island where this occurs is Andros Island, The Bahamas where the base of the lens is truncated near the interface between the upper low hydraulic conductivity layer and a lower high hydraulic conductivity layer (Ritzi et al. 2001). The truncation of the freshwater lens for Bahama-type islands has also been studied using analytical equations by Vacher (1988), who showed that there is greater truncation of the lens with an increasing difference in hydraulic conductivity between the two layers.

In an aquifer with a low hydraulic conductivity upper layer and high hydraulic conductivity lower layer, the greater the thickness of the upper layer, the greater the freshwater lens volume. As the difference in hydraulic conductivity between the layers increases, there is a greater decrease in the freshwater lens volume. Ketabchi et al (2014) developed an analytical model for a circular Bahamas-type island. They also used numerical simulations to evaluate the impact of the sharp interface assumption which was used in the derivation of the analytical model. Since the analytical solution neglected dispersion, the fresh groundwater lens thickness for a two layer Bahamas-type island was

overestimated compared to the numerical model. Additionally, the models were used to perform a sensitivity analysis of several hydrologic parameters to compare the impact of land surface inundation on the depth of the freshwater lens. Among the parameters that were investigated, layer properties were one of the most significant in governing the freshwater lens response to sea level rise. This includes the layer thickness and the difference in magnitude in hydraulic conductivity between the upper and lower layers. For Ketabchi et al's simulations, a one- and two-order magnitude difference in K between layers resulted in a 6% and 11% decrease in the freshwater lens volume respectively compared to the homogeneous case. While the analytical model is a useful tool and the results show the freshwater lens is more sensitive to aquifer properties than to sea level rise, the simulations do not show the evolution of the lens overtime or address groundwater inundation.

Dose et al (2014) compared steady state freshwater lens shape and flow patterns using analytical solutions from Fetter (1972) and Vacher (1988), numerical and physical models for common distributions of hydraulic conductivity and recharge patterns for islands modified from Vacher and Wallis (1992) including the Bahamas-type island. One notable observation from the steady state numerical and physical models of the Bahamas-type island was that there are two types of flow paths; flow that only occurs in upper layer and flow that passed to lower layer and traveled laterally. The velocity in the lower unit was much higher compared to the upper unit due to the higher hydraulic conductivity. In terms of performance among the different modeling methods, the numerical simulations were in good agreement with the physical model results. The analytical solution of Fetter (1972), however, didn't capture the interface dynamics along the transition zone of the freshwater lens and while the general shape of the lens for Vacher (1988) was matched numerical and physical modeling results, the depth to the base of the freshwater lens was significantly underestimated. Of the three different modes of modeling, numerical modeling lends itself to being a useful tool to investigate a Bahama-type island (Dose et al. 2014). While Dose et al (2014) focus on how to represent different hydrogeologic settings, they do not compare their results to a homogeneous base case or investigate the impacts of sea level rise and groundwater inundation.

While there have been several studies that look at the impact of sea level rise on groundwater inundation (Rotzoll and Fletcher 2013; Hoover et al. 2017; Cooper, Zhang, and Selch 2015; Habel et al. 2017; Masterson et al. 2014; Gulley et al. 2016; Mancewicz et al. 2023) there have been very few that also consider the impact of heterogeneity in hydraulic conductivity and directly include surface water/groundwater interactions (Terry and Chui 2012). Terry and Chui (2012) used a numerical model to simulate an atoll island and examine the effects of long term sea level rise and wave washover events from tropical cyclones. The model domain includes a swamp at the center of the island and a shallow, high hydraulic permeability upper layer and a low hydraulic conductivity lower layer with one order of magnitude difference in hydraulic conductivity between the two. For an increase in sea level of 20cm and 40cm, the freshwater lens decreased by 20-25% and 50% respectively. Additionally, as sea level rises the pressure difference between the lake and the aquifer becomes much smaller and allows for the saline ocean water to

intrude creating an area of brackish water underneath the swamp. In their simulations, including two geologic layers does not appear to notably impact the results, as there was no specific discussion on how the layering attributed to the observed response of the freshwater lens to sea level rise. While the idealized atoll island represented in these simulations is similar to the Bahamas-type island, the implementation of the boundary conditions was somewhat simplified. For example, the surface water feature (swamp) was represented as a specified head boundary and the salinity was kept constant during the sea level rise simulations. This representation does not allow for changes to the salinity of the swamp or the effects of changing salinity on the interactions between the swamp and the aquifer. Additionally, sea level rise was represented as instantaneous sea level rise and does not take into consideration the dynamics of how the freshwater lens evolves overtime.

In this paper, we use finite difference numerical variable density groundwater flow and transport simulations to evaluate the impact of groundwater inundation due to sea level rise for a Bahamas-type island. We compared the results of a homogeneous base case to simulations with two layers of hydraulic conductivity in various hydrogeologic settings, including the order of magnitude difference in hydraulic conductivity between the two layers, the depth to the layer interface, lake evaporation rate and sea level rise rate. The results examine the impact that the two layer aquifer configuration has on freshwater lens dynamics and lake-aquifer interactions.

3.2 Methods

We used MODFLOW6 (Langevin et al. 2017) to run 2D steady state and sea level rise idealized island simulations for a range of hydraulic conductivity configurations, net lake evaporation rates, and sea level rise rates, summarized in Table 1 and Table 2. MODFLOW6 is an object-oriented based variable density groundwater flow and solute transport model and is the most recent core version of MODFLOW, a widely used groundwater numerical modeling program maintained by the U.S. Geological Survey. We ran all of our simulations on Michigan Technological University's High Performance Computing Shared Facility. We used FloPy (Bakker et al. 2021), a python library for the MODFLOW suite of programs, to create input files, run the model, and post process results. Simulating idealized conditions allows us to focus on certain processes and properties in an isolated manner that might otherwise be obscured in a more complex system.

We ran homogeneous simulations and simulations that had two horizontal layers of differing hydraulic conductivity, similar to the geologic conditions encountered throughout the Bahamas. For our study, the hydraulic conductivity for the homogeneous aquifer simulations was set to 10 m/d. For the layered simulations, the hydraulic conductivity of the upper layer was fixed at 10 m/d down to a depth of approximately -20m and -15m relative to sea level (0m) for the layer base case and the deeper layer interface depth case, respectively. For all simulations the bottom depth of the domain was -80.35m. The hydraulic conductivity of the lower layer was varied and set to 100, 1000, and 10000 m/d providing a corresponding one, two and three order of magnitude

difference in hydraulic conductivity between the upper and lower layer. These values of hydraulic conductivity are typical for carbonate islands in the Bahamas where the range of maximum and minimum effective hydraulic conductivity from pump tests are on the order of 10^4 and 10^{-2} m/d respectively (Whitaker and Smart 1997). Additionally, the average hydraulic conductivity from pump tests is on the order of 10^1m/d for the upper layer and, 10^3 m/d for the lower layer (Whitaker and Smart 2000), while Breithaupt et al. (2021) reports up to a four order magnitude difference in permeability between the upper and lower layer on San Salvador Island, the Bahamas derived from tidal data analysis. Due to the assumption of symmetry, only half of the 1000m wide island was represented in the model domain.

A no flow boundary condition was used on the left side and along the bottom of the model domain. A general head boundary is used to represent the ocean along the right hand side of the domain with a constant salinity of 35 g/L, equal to that of seawater. A general head boundary was used instead of a constant head boundary because of the implications for solute transport. With a constant head boundary, the constant solute concentration would be specified for the groundwater cell itself, as opposed to an external source. It can be difficult to generate a freshwater outflow face when using the constant head boundary because this boundary condition requires that the constant concentration is specified for the actual grid cell as opposed to some external source.

A 50m wide area of low topography is located in the center of the island (left hand side of the model domain), which floods when sea level forces the water table to rise above the bottom of the depression. Once the water table intersects the land surface in the low topography area, the Lake Package and the Lake Transport Package are “turned on” within MODFLOW 6. As the lake continues to expand laterally, the Lake Package automatically reassigns the boundary conditions for the newly flooded cells, transforming them from acting as “aquifer cells”, to acting as “lake cells”. Using these two MODFLOW packages to represent groundwater inundation is further described in Mancewicz et al 2022.

Steady state spin-up simulations were used to generate the initial conditions for the sea level rise simulations for the homogeneous and layered cases, where the initial position of the water table was located just beneath the area of low topography at an elevation of 0.64m. For the steady state simulations, the general head boundary (sea level) is set to a constant value of 0m elevation. We specified net recharge (precipitation minus evapotranspiration) for the aquifer and net lake evaporation (precipitation minus evaporation) for the lake. Throughout the Bahamas, the potential evapotranspiration (PET) and rainfall respectively vary from 140 cm/yr and 150 cm/yr in the north to 160 cm/yr and 75 cm/yr in the south (Gulley et al. 2016). While the net annual water budget for some of these islands is negative, on a monthly basis the aquifers experience seasonal recharge. For our study, the net land surface recharge remained fixed for all simulations at 20 cm/yr, similar to literature values (Gulley et al. 2016). We used net lake evaporation rates of 1.5 and 3.0 times the amount of net recharge (30cm/yr and 60cm/yr respectively) based on PET to explore the impact of evaporation rate on lake-groundwater interactions.

For the sea level rise simulations, we used two sea level rise rates (1m/100 years, 2m/100 years) which fall within the range of predicted end of century sea level rise rates in the Caribbean (Sweet et al. 2017). The head for the general head boundary condition was linearly increased each timestep. The sea level rise simulations occurred over a 60-year period with daily timesteps. Coastal inundation was not included in these simulations so that we could isolate the impact of groundwater inundation on the island's hydrogeology. In summary, we simulated a combination of one homogeneous and three layered systems, two-layer interface depths, two net lake evaporation rates, two net recharge rates and two sea level rise rates, for a total of 32 simulations (Table 1).

Table 1: Description of two layer and homogeneous simulations.

Name	**Hydraulic conductivity distribution**	**Depth to layer interface**	**Evaporation**	**Recharge**	**SLR rate**
S1-1	10/100	base	high	base	low
S1-2	10/100	base	high	base	high
S1-3	10/100	base	high	low	low
S1-4	10/100	base	high	low	high
S1-5	10/100	shallow	high	base	high
S1-6	10/100	shallow	low	base	low
S1-7	10/100	shallow	high	low	high
S1-8	10/100	shallow	low	low	low
S2-1	10/1000	base	high	base	low
S2-2	10/1000	base	high	base	high
S2-3	10/1000	base	high	low	low
S2-4	10/1000	base	high	low	high
S2-5	10/1000	shallow	high	base	high
S2-6	10/1000	shallow	low	base	low
S2-7	10/1000	shallow	high	low	high
S2-8	10/1000	shallow	low	low	low
S3-1	10/10000	base	high	base	low
S3-2	10/10000	base	high	base	high
S3-3	10/10000	base	low	base	low
S3-4	10/10000	base	low	base	high
S3-5	10/10000	base	high	low	low
S3-6	10/10000	base	high	low	high
S3-7	10/10000	shallow	high	base	low
S3-8	10/10000	shallow	high	base	high
S3-9	10/10000	shallow	high	low	low
S3-10	10/10000	shallow	high	low	high
SH-1	homogeneous	-	high	base	low

SH-2	homogeneous	-	high	base	high
SH-3	homogeneous	-	low	base	low
SH-4	homogeneous	-	low	base	high
SH-5	homogeneous	-	high	low	low
SH-6	homogeneous	-	high	low	high

Table 2: Values for descriptions used in defining simulation scenarios

Parameter	**Description**	**Value**	**Units**
Depth to layer interface	base	20	m elevation
	shallow	15	m elevation
Net evaporation	high	0.00165	m/d
	low	0.00083	m/d
Net recharge	base	0.00055	m/d
	low	0.00028	m/d
SLR rate	high	2	m/100 yr
	low	1	m/100 yr

In order to determine the impact of a two-layer case on lake salinity and freshwater lens extent, we examined the lake salinity over time, cross section figures of aquifer salinity, and the extent of the freshwater lens. An aquifer grid cell is considered to contain freshwater if the salinity is ≤ 1.0 g/L. The extent of the freshwater lens is defined as the percent difference compared to the initial conditions. The total number of freshwater grid cells for a given timestep was divided by the number of freshwater grid cells in the initial conditions. At the start of the sea level rise simulation the percent of the initial freshwater lens volume is 100% and as sea level rises, the extent of the freshwater lens and the percentage decreases.

After providing an overview of the various scenarios, we looked at a subset of the results that fall into one of two end member cases for the homogeneous and layered simulations with the three order of magnitude difference in hydraulic conductivity. The first end member case is the “freshwater limited” case (SH-6 and S3-10), which consists of high evaporation rate, low recharge, high SLR rate, and a shallow depth to the interface for the layered scenario. This set of parameters has the potential to more significantly limit the extent of the freshwater lens. The second case is the “freshwater abundant” case (SH-3 and S3-3) which consists of the low evaporation rate, high recharge, low SLR rate and the base depth to the interface for the layers scenario. For this case, it is expected that the freshwater lens will be impacted to a lesser extent.

3.3 Results

Both the initial and final size of the freshwater lens varies between the homogeneous and layered cases. This is illustrated in Figure 1 which shows several panels each with a cross

section view of the groundwater salinity. The low-lying depression, which floods to become a lake, is shaded in black on the upper left side of each panel and the ocean boundary is on the right side. Row A shows the initial conditions for Row B (shallow depth to interface, high evaporation, low recharge, high SLR rate). Row C contains the initial conditions for Row D (shallow depth to interface, high evaporation, base recharge, high SLR rate). Row E contains the initial conditions for Row F (base depth to interface, high evaporation, base recharge, low SLR rate) and Row G (base depth to interface, high evaporation, base recharge, high SLR rate).

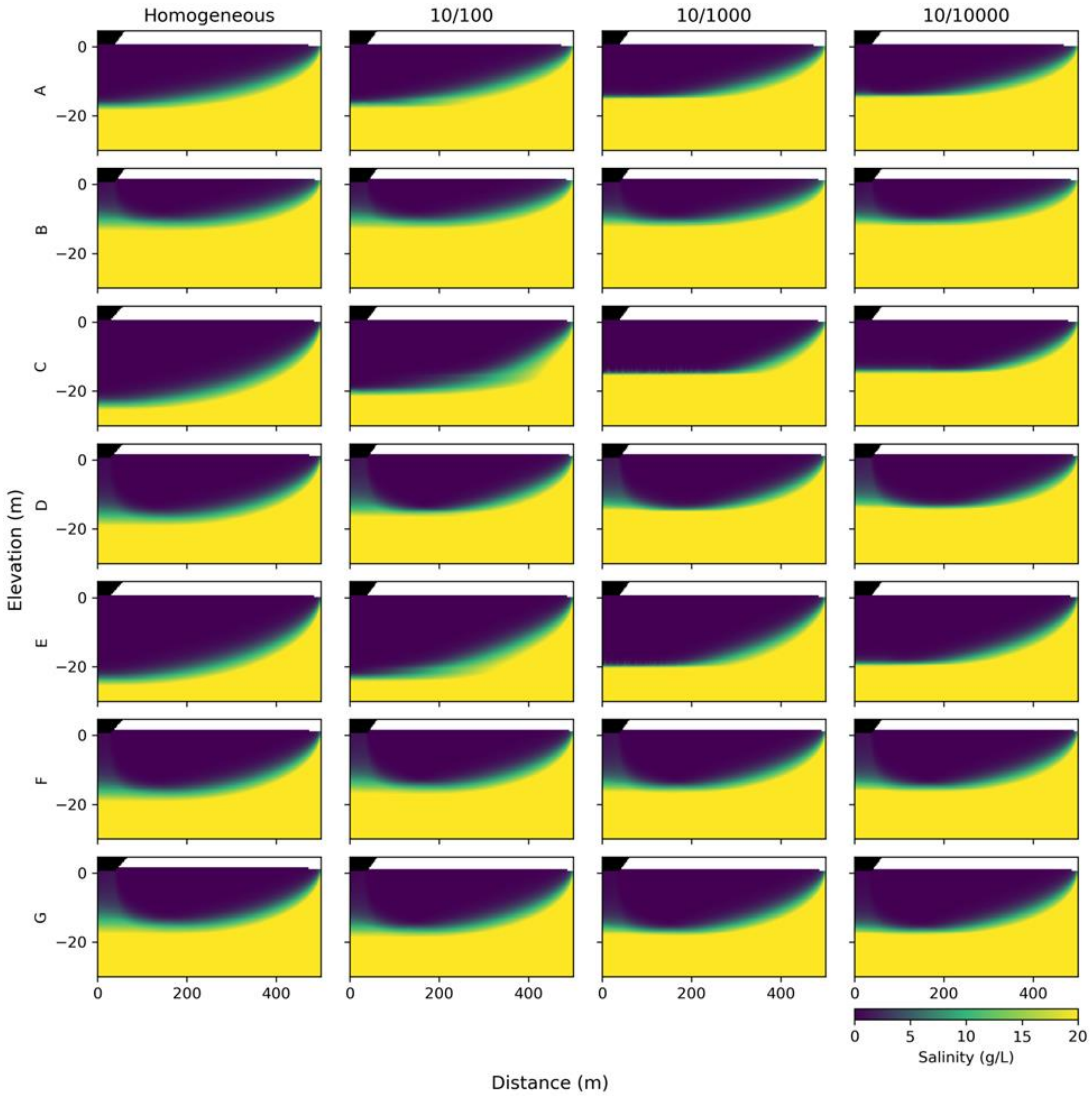

Figure 1: Cross section of groundwater salinity for selected simulations. Row A contains the initial conditions for Row B (shallow depth to interface, high evaporation, low recharge, high SLR rate). Row C contains the initial conditions for Row D (shallow depth to interface, high evaporation, base recharge, high SLR rate). Row E contains the initial conditions for Row F (base depth to interface, high evaporation, base recharge, low SLR rate) and Row G (base depth to interface, high evaporation, base recharge, high SLR

rate). The lake is located as the black area in the upper left and the ocean boundary is on the righthand side. The freshwater lens is shown in dark blue and the transition zone is in green. The freshwater lens is truncated at the layer boundary for the layered cases and results in a smaller freshwater lens compared to the homogeneous case.

The initial conditions (Row A, Row C and Row E in Figure 1) show subtle differences in the extent of the freshwater lens across the different hydraulic conductivity configurations. The largest freshwater lens occurs for the homogeneous case, where the base of the lens is not subject to truncation by the interface between two layers. The greatest difference in the extent of the freshwater lens overall between the homogeneous and layered case is along the transition zone of the freshwater lens. The transition zone is thicker for the lower order of magnitude difference in hydraulic conductivity between the upper and lower layer. The greater the difference in hydraulic conductivity between the upper and lower layer, the smaller the transition zone and the sharper the salinity contrast between the freshwater lens and the surrounding higher salinity groundwater.

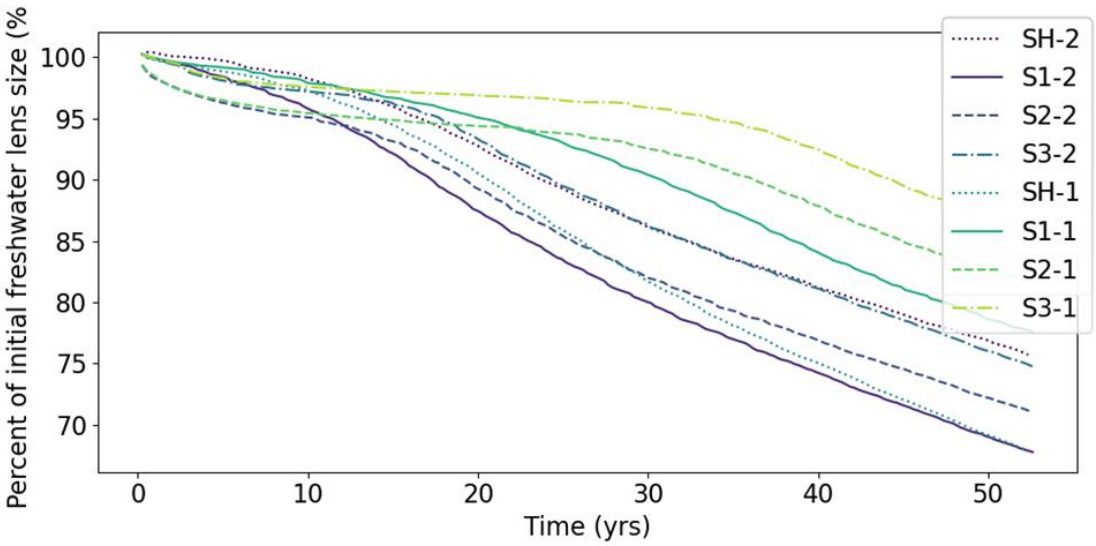

Figure 2: Change in the extent of the freshwater lens as the percent difference between the number of freshwater grid cells at the beginning of the simulaiton and the end. The dotted, solid, dashed, and dot dash curves are for the homogeneous, one order, two order and three order magnitude difference in layer hydraulic conductivity respectively. Both a low and high SLR rate simulation are shown for base depth to layer interface, high evaporation, and the base recharge rate. The long term rate of change in size of the freshwater lens is the same for a given set of parameters, regardless of the sea level rise rate.

For a fixed hydrogeologic setting, after an initial response of the freshwater lens to sea level rise and the lake “turning on”, the change in the freshwater lens occurs at a constant rate that is the same regardless of SLR rate. This is shown in Figure 2, where the change to the freshwater lens over time is shown for the homogeneous and layered cases with the base depth to layer interface, high evaporation, and the base recharge rate for both the

high and low sea level rise rate. The curves for the percent difference in the freshwater lens for the high and low SLR rate are eventually parallel for a given hydraulic conductivity distribution, with the overall reduction in the size of the freshwater lens for the high SLR rate is greater than for the low SLR rate. Overall, the homogeneous case shows the greatest reduction in the extent of the freshwater lens, while the three order of magnitude layered hydraulic conductivity configuration shows the smallest change. This is illistrated in Figure 2 and also shown in Table 3. In the area underneath the lake, upconing occurs to meet the evaporative demand from the lake. For the homogeneous case, there is greater salinization due to upconing compared to the layered cases, as seen in Figure 1. In the layered case, the lower hydraulic conductivity in the upper layer limits the amount of upconing and delays further salinization of the aquifer. The difference in results between the layered and homogeneous case is greatest for the three order of magnitude difference in hydraulic conductivity between the upper and lower layer. Because of this, the homogeneous and layered case with three order of magnitude difference in hydraulic conductivity between the upper and lower layer were selected as a subset of the results for further analysis in section 3.3.2 Comparison of end member cases.

Table 3: Results for each simulation including the lake salinitiy at the end of the simulation, number of freshwater cells at the start and end of the simulation, and the percent difference in the number of freshwater cells over the duration of the simulation.

Name	**Final lake salinity (g/L)**	**Starting number of freshwater cells**	**Final number of freshwater cells**	**Percent difference in the number of freshwater cells (%)**
S1-1	2.36	17281	13354	77.45
S1-2	4.15	17278	11671	67.69
S1-3	0.58	12016	9951	83.26
S1-4	3.05	12012	8162	68.29
S1-5	5.48	16119	11798	72.92
S1-6	0.08	16105	14321	88.51
S1-7	2.06	12748	8553	67.16
S1-8	0.23	12763	10369	81.42
S2-1	1.54	16861	13837	81.56
S2-2	3.40	16850	12042	70.98
S2-3	0.42	12070	10245	85.27
S2-4	2.65	12067	8390	69.83
S2-5	6.86	14544	11444	75.95
S2-6	0.18	14542	13065	86.71
S2-7	1.70	12569	8889	70.82
S2-8	0.01	12575	11303	90.06
S3-1	1.29	16187	13839	85.67
S3-2	3.34	16186	12062	74.67

S3-3	0.03	16187	15277	94.58
S3-4	0.09	16186	14594	90.35
S3-5	0.48	12183	10055	83.01
S3-6	2.66	12180	8323	68.71
S3-7	1.62	13758	12225	88.84
S3-8	7.42	13761	11154	81.06
S3-9	0.15	12267	10685	87.38
S3-10	1.73	12257	8855	72.42
SH-1	3.62	17824	12055	67.58
SH-2	1.38	17910	13477	75.55
SH-3	0.11	17824	14112	79.11
SH-4	3.54	17824	12043	67.51
SH-5	0.24	12835	10492	82.09
SH-6	1.94	12832	8792	68.79

3.3.1 Initial conditions

The most significant factor regarding the impact of groundwater inundation on the extent of the freshwater lens and lake salinity is the initial conditions, regardless of the hydraulic conductivity configuration. The differences in the properties that determine the initial conditions amongst the different scenarios ultimately govern the response of the freshwater lens and lake salinity to sea level rise and groundwater inundation. The recharge and, for the layered cases, the depth to the interface and order of magnitude difference in hydraulic conductivity between the upper and lower layer are the parameters that determine the initial freshwater lens extent.

In general, for the properties that determine the initial conditions for the layered cases the freshwater lens is truncated at the interface between the high and low hydraulic conductivity layers (Figure 1). By decreasing the depth to the interface, the truncation is shallower and reduces the depth to the base of the freshwater lens for the layered cases by 5 – 32% compared to the homogeneous case. The percent difference in the depth of the base of the freshwater lens between the layered and homogeneous case is greatest for the three-order difference in hydraulic conductivity. The difference is greater for the three-order difference in hydraulic conductivity between the upper and lower layer because the effects of truncation of the lens are more pronounced for the higher order differences in hydraulic conductivity. For the effects of recharge rate on the initial conditions, decreasing the recharge results in a shallower depth to the base of the freshwater lens. The freshwater that makes up the freshwater lens only comes from land surface recharge. When the recharge rate is lower, there is less freshwater and a smaller freshwater lens for both the homogeneous and layered cases.

The impact of the depth to the interface between the two layers on differences in the initial conditions between the layered and homogeneous cases varies depending on recharge rate. A shallower interface between the layers reduces the freshwater lens depth

overall and additional changes in recharge have a minimal influence on the depth of the freshwater lens. The greatest percent difference in the depth to the base of the freshwater lens between the homogeneous and layered cases occurs for the layered cases with base recharge rate and a shallow interface depth, which ranges from 10 – 32% and increases with increasing order of magnitude difference in hydraulic conductivity between the layers. The depth of the layer interface truncates the freshwater lens for the layered cases, which the homogeneous case is not subject to. When comparing the effects of the base versus the low recharge rate, there is relatively little impact on the difference between the homogeneous and the layered cases. For the base interface depth cases with the base recharge rate, the percent difference between the homogeneous and layered is <14% for all layered cases. For the base interface depth cases with a low recharge rate, the percent difference between the homogeneous and layered case is <8%.

3.3.2 Comparison of end member cases

For the "freshwater limited" scenarios, there was only a slight difference between the three-order of magnitude layered case and the homogeneous case for the final extent of the freshwater lens and lake salinity. The variation in the final percent difference in the freshwater lens at the end of the simulation is a function of the initial conditions. There is only a 0.7% difference in the number of freshwater cells at the end of the simulation between the three-order difference layered case and homogeneous case (Figure 3), but a percent difference of 5% in the final extent of the freshwater lens (Table 3). There is a greater difference in the extent of the freshwater lens for the homogeneous case despite having a similar final number of freshwater cells as the layered cause because the layered case starts out with 500 fewer freshwater cells to begin with, so the overall change for the layered case is not as great.

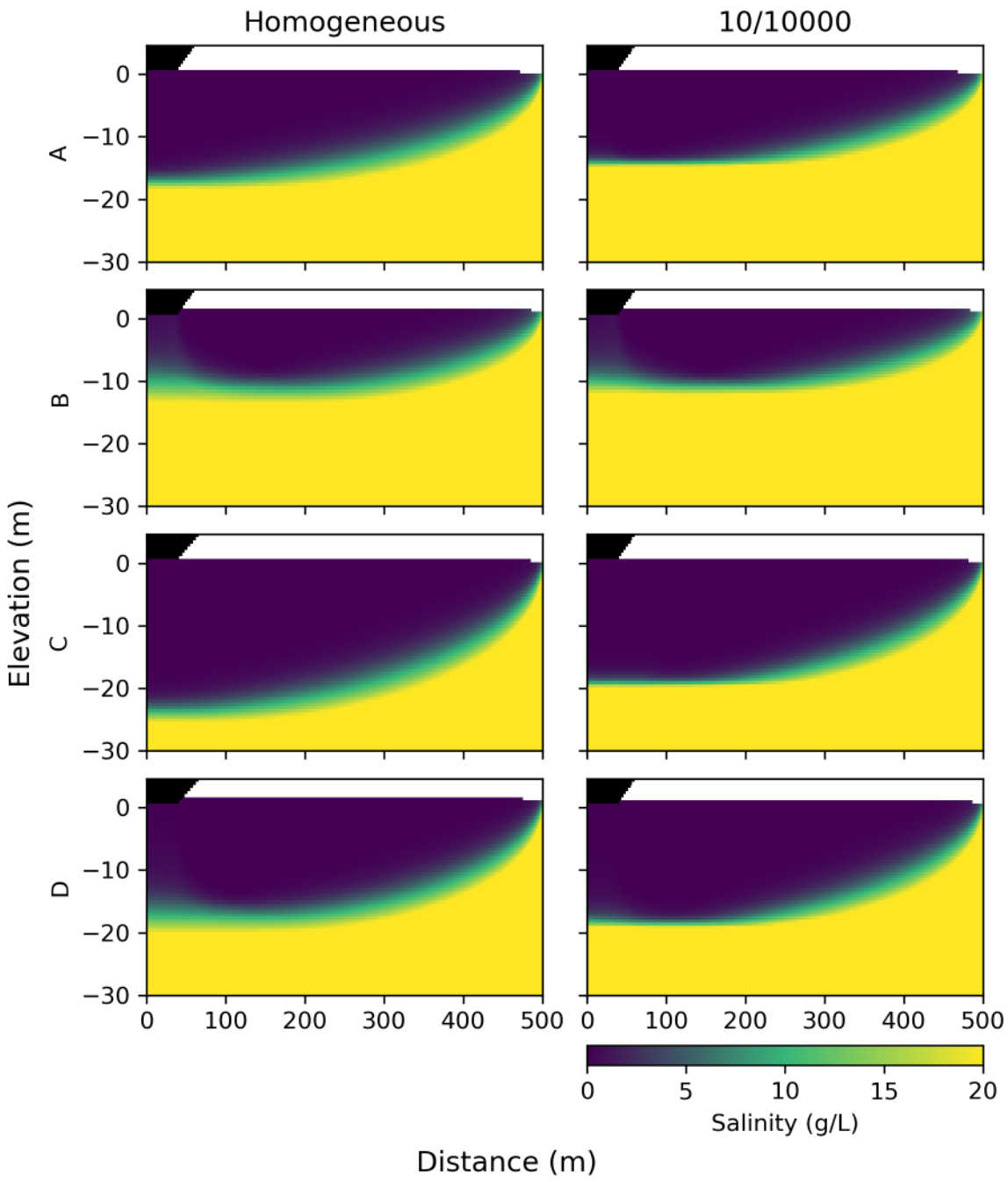

Figure 3: Cross section of groundwater salinity for selected simulations. Row A contains the initial conditions for the final timestep of simulations in Row B ("freshwater limited" cases). Row C contains the initial conditions for the final timestep of simulations in Row D ("freshwater abundant" case). The lake is located as the black area in the upper left and the ocean boundary is on the righthand side. The freshwater lens is shown in dark blue and the transition zone is in green. There is less of a difference between the

homogeneous and layered case for the “freshwater limited” case compared to the “freshwater abundant case.”

The final lake salinity at the end of the simulation for the “freshwater limited” case only differs by 0.2g/L between the homogeneous and three order magnitude layered scenarios (Table 3). The small difference in lake salinity is a function of the salinity of the inflowing water to the lake. With the homogeneous simulation, there is greater upconing of the freshwater lens underneath the lake. As the salinity of the water flowing into the lake from this area increases over time, so does the lake salinity. In comparison for the layered case, the upconing is limited by the low hydraulic conductivity and the area underneath the lake remains relatively fresh compared to the homogeneous simulation. Consequently, the water that flows into the lake from this area is also of a relatively low salinity and the overall lake salinity increases less than for the homogeneous case.

For the “freshwater abundant” scenarios, there are much more notable differences in the final extent of the freshwater lens between the layered and homogeneous scenarios, while the lake salinity remains similar between the two setups. The two-layer scenario starts off with 10% fewer freshwater cells than the homogeneous simulation due to the truncation of the freshwater lens along the transition zone between the upper and lower layer (Figure 3). The number of freshwater cells at the end of the homogeneous simulation is 22% fewer than the two-layer simulation. The difference in the number of freshwater cells over the course of the simulation is relative to the initial conditions. The homogeneous simulation had a greater reduction in the number of freshwater cells, but the two-layer simulation had fewer cells to start with, so the additional effects of sea level rise are less intense compared to the hydrogeologic conditions that govern the initial conditions of the freshwater lens prior to sea level rise.

The final lake salinity at the end of the simulation for the “freshwater abundant” case remain <1 g/L for both the homogeneous and two-layered case which have a final lake salinity of 0.81 g/L and 0.03 g/L respectively (Table 3). The low evaporation rate for the “freshwater abundant” case causes less evapoconcentration compared to the “freshwater limited” case, as well as less upconing of higher salinity water underneath the lake, both of which result in a lower lake salinity. Additionally, the higher recharge rate compared to the “freshwater limited” case provides a greater freshwater lens to start with, prior to the effects of sea level rise or groundwater inundation, resulting in a low lake salinity for both the homogeneous and layered scenarios.

3.4 Discussion

When determining which properties of the homogeneous and layered scenarios govern the response of the freshwater lens and lake salinity, ultimately it is the properties that determine the initial conditions, not any set of associated with the transient SLR simulations. For our simulations, the initial conditions determine the trajectory of the final freshwater lens and lake salinity at the end of the simulation. The initial extent of the freshwater lens depends on both the recharge and the hydraulic conductivity configuration. Therefore, as an application to island freshwater management, it is

important to have a good understanding of the properties that govern the initial conditions for a conceptual model, as this will ultimately determine the impact of sea level rise and groundwater inundation on the freshwater. Additionally, after an initial response of the freshwater lens to sea level rise and the lake being "turned on", for a given set of parameters the rate of freshwater lens depletion was the same regardless of sea level rise rate.

One limitation in this work is that for the layered simulations, the hydraulic conductivity for each layer was assumed to be homogeneous and isotropic. This simplification allowed us to look at the fundamental relationships between different hydrogeologic parameters and the impact of groundwater inundation on the freshwater lens and lake salinity. However, it has been shown that vertical connectivity, such as caves or conduits, can exist between the upper low hydraulic conductivity layer and the underlying high hydraulic conductivity layer, providing a direct hydrologic connection to the ocean (Breithaupt et al 2021). Future work could include incorporating heterogeneity in the vertical hydraulic conductivity to explore a more complex conceptual model. Additionally, our simulations neglected any impact of tidal or seasonal variation in sea level rise. It is expected that if additional mixing from any of these sources was included, it would enhance further loss of the freshwater lens and contribute to increasing lake salinity. It is also likely that the impact would be similar for both the layered and the homogeneous case. It should be noted that relative SLR rates for atoll islands can differ significantly compared to tectonically stable carbonate platform islands of the Bahamas, as subsidence and island building processes contribute to the overall relative SLR rate (Woodroffe 2011; Masselink, Beetham, and Kench 2020; Duvat 2019).

3.5 Conclusion

Groundwater inundation due to sea level rise poses a significant threat to the extent of the freshwater lens on islands. One common geologic configuration for islands, especially in the Caribbean, is for there to be a high hydraulic conductivity layer that underlies an upper low hydraulic conductivity layer. We performed a sensitivity analysis to compare the impact of sea level rise and groundwater inundation on the freshwater lens and lake salinity for a homogeneous and layered aquifer. For two end member cases, the difference between the layered scenario and homogeneous scenario was more pronounced for the "freshwater abundant" case due to the greater difference in the starting extent of the freshwater lens. Ultimately, the extent of the freshwater lens at the end of the simulation was strongly dependent on the initial conditions. When considering the impacts of sea level rise and groundwater inundation on the freshwater lens, it is essential to have a good understanding of the initial conditions, regardless of whether the aquifer is represented as a two-layer system or homogeneous.

4 Chapter 4: Density driven instabilities due to groundwater inundation from sea level rise may threaten island freshwater lens

4.1 Introduction

Groundwater inundation due to sea level rise is a threat to fresh groundwater resources, especially in an island setting, and could also create conditions that lead to density-driving fingering events, further salinizing the groundwater. As sea levels rise, the freshwater lens on islands also rises or "floats" upward due to the difference in density between the freshwater lens and surrounding saline groundwater. As the groundwater table rises, it may intersect the land surface in low lying areas creating or expanding surface water features such as lakes or wetlands (Rotzoll and Fletcher 2013; Masterson et al. 2014; Habel et al. 2017; Gulley et al. 2016; Mancewicz et al. 2023). Freshwater that was once stored underground in the aquifer is now exposed to additional evaporative losses depleting the freshwater lens (Gulley et al. 2016; Mancewicz et al. 2023).

In general, the lake receives incoming water from groundwater flow and precipitation, while water is lost from the lake via evaporation. Higher evaporation rates, especially when evaporation exceeds incoming precipitation, can result in upconing of the freshwater lens underneath the lake (Vacher and Wallis 1992). Additionally, the loss of freshwater from evaporation can also concentrate the solutes within the newly formed lake. As the salinity of the lake increases due to evapoconcentration, there is a greater difference in salinity, and consequently density, between the lake and the underlying aquifer. This density gradient could cause instabilities which "superimpose perturbations on the evolving concentration distributions" (Schincariol, Schwartz, and Mendoza 1994). If the perturbation continues to grow, the groundwater system is considered unstable and a finger-like plume of more dense water will intrude into the underlying lower density groundwater (Schincariol, Schwartz, and Mendoza 1994).

Wooding et al (1997) investigated such a case for the generalized salt lake scenario, where a lake is represented by two end members; either a "dry" salt lake due to extensive evaporation, or a saline ponded surface. The authors used linear stability analysis to investigate the stability of the saline boundary layer that develops at the land surface due to evaporation and used Hele-Shaw cell experiments and numerical simulations to evaluate the parameters that govern the onset of density dependent fingering. They found that the boundary layer Rayleigh number, used to describe onset of instability, is inversely proportional to the lake evaporation rate, and directly proportional to permeability, suggesting the importance of these two parameters in governing the behavior of density dependent fingering (Wooding, Tyler, and White 1997).

The occurrence and onset of density driven fingering has been studied not only in regard to the presence of a hypersaline lake (Wooding, Tyler, and White 1997, Simmons et al 1991), such as those occurring on small islands (Juster et al. 1997), but in other coastal settings as the result of tidal flooding (Greskowiak 2014; Wu et al. 2022) or storm surge (van Duijn, Pieters, and Raats 2019; Post and Houben 2017). Density driven fingering

events can play a strong role in controlling groundwater solute transport and flow patterns, as shown by Post and Houben (2017), who analyzed historic salinity measurements from storm driven flooding on a German barrier island. The authors used numerical modeling to explore the role of density driven fingering on the observed downward movement of seawater following the inundation by evaluating the importance of numerical and hydrogeologic properties. The results indicate that density driven fingering was a key process in explaining the sequence of observed salinity trends. Initially, the density gradient drives downward flow of fingering plumes. The density gradient is then reduced due to dispersion and further solute transport occurs via advection. Density driven flow was shown to be more significant in governing the response of saltwater intrusion than several other factors investigated including lateral groundwater flow, incorporating transient recharge, or using a 2D versus a 3D grid (Post and Houben 2017).

There is also field data that provides evidence of density driven fingering events occurring underneath a hypersaline pond on Cluett Key, Florida, a carbonate mud island composed of an upper thin low hydraulic conductivity mud layer underlain by high hydraulic conductivity limestone (Juster et al. 1997). Observation data demonstrate a process that the authors referred to as reflux, which occurs when the salinity of ponded water is concentrated by evaporation and then sinks into underlying less dense groundwater (Juster et al. 1997). The hypersaline water that is lost from the pond is replaced by an influx of less dense seawater that comes up from the contact between the mud and limestone. As the hypersaline plume is dispersed due to horizontal flow, the salinity underneath the pond is once again at saltwater concentrations and the process restarts, as evaporation concentrates the solutes in the pond leading to hypersaline conditions (Juster et al. 1997). The authors state that this process could continue "indefinitely" as the pond continues to undergo evapoconcentration and maintain hypersalinity, and the dispersion in the aquifer continues to disperse the intruding plume, resetting the lower aquifer salinity and the density gradient between the pond and underlying aquifer (Juster et al. 1997).

The onset and occurrence of density driven fingering is affected by hydraulic conductivity and mixing. Using a modified version of the Elder problem, Xie, Simmons, and Werner (2011) found that the speed of density driven fingers is a linear function of permeability; as permeability increased by an order of magnitude, so did the downward velocity of the fingers. Liu and Tokunaga (2020) performed a sensitivity analysis of many different hydrogeologic parameters to classify flow and solute behavior of 2D simulations where solute was injected along a portion of the upper boundary and constant head was boundaries were used on the right and left edges of the domain to induce a horizontal hydraulic gradient, with a no flow boundary elsewhere. Increasing the hydraulic conductivity shifted the behavior from vertical hydraulically driven flow to a mixed regime where density driven flow becomes increasingly dominant. Further increasing the hydraulic conductivity enhanced the horizontal hydraulically driven flow, replacing the vertical hydraulically driven flow as a key driver in the mixed regime (Liu and Tokunaga 2020). However, incorporating heterogeneity of hydraulic conductivity of

the aquifer did not affect the regimes much because it did not significantly change the driving forces (Liu and Tokunaga 2020).

Incorporating a lower hydraulic conductivity layer, such as lakebed sediments between a ponded surface and an underlying aquifer, can act as a barrier, preventing intrusion of the salt finger into the aquifer below (van Duijn, Pieters, and Raats 2019). In general, lakebed sediments play a significant role in governing the flow between a hypersaline lake and underlying aquifer with regard to solute flux (Sheibani et al. 2020). Greater sediment thickness and a low aquifer hydraulic conductivity can prevent nearly all incoming salt flux from a hypersaline lake to the underlying aquifer (Sheibani et al. 2020). Wu et al. (2022) looked at the onset of density driven fingering in the case of a stratified salt marsh where tidally driven flooding of the marsh platform, which consisted of an upper mud layer of low hydraulic conductivity and an underlying higher hydraulic conductivity sand aquifer, could result in fingering events. As the hydraulic conductivity of the mud layer was decreased, it took longer before the onset of fingering and the fingers were smaller and denser. This was attributed to the decrease in advection because of the lower hydraulic conductivity in the mud layer (Wu et al. 2022).

In the case of Xie, Simmons, and Werner (2011)modified Elder problem, increasing the porosity, resulted in a decrease in the velocity of the finger plume. Changes to dispersivity, however, did not significantly impact the finger plume velocity, but did impact the shape of the fingers. Reducing the transverse dispersivity resulted in narrower fingers and increasing the longitudinal dispersivity increased the vertical spread, with fingers looking more “balloon shaped” (Xie, Simmons, and Werner 2011). For a sensitivity analysis on the stability of an upper saline plume that overlies a submarine groundwater discharge zone, increasing the longitudinal dispersivity by a factor of four reduced the number of salt fingers and caused significant “smearing” along the saltwater/freshwater interface (Greskowiak 2014), while low dispersion may allow instabilities to form more easily (Schincariol et al 1994). For numerical modeling of the barrier island by Prost and Houben (2017) mentioned above, dispersion of solutes reduces the density gradient, and transport of solutes goes from density driven vertical downward movement to lateral advection driven transport. The density gradient drives downward flow of fingering plumes, but as dispersion occurs, there is less of a gradient in density (and less of a driving force for downward density driven flow). Instead, further solute transport occurs via advection (Prost and Houben 2017).

The behavior of the fingering event is also impacted by incoming fresh and/or saltwater fluxes. In the case of Lui and Tokunaga’s (2020) sensitivity analysis, increasing the solute injection rate, source concentration and injection length all shift the behavior towards the density driven flow regime and became increasingly unstable. In Wu et al, (2022), as the difference in concentration between the inundating seawater and underlying groundwater decreases, it took longer for fingering to occur. Schincariol et al (1994) also found that the greater the density gradient, the more likely that instabilities are to occur. Greskowiak (2014) used 2D numerical model simulations to perform a sensitivity analysis to examine the presence of DF events from tidal fluctuations in coastal areas and the impact on submarine fresh groundwater discharge. A constant

concentration freshwater specified flux boundary was used for landside edge of the domain. For the case with a reduced incoming freshwater flux, there were no density driven fingering events, even though it might be expected that a lower freshwater flux would allow for finger formation because of a reduction in advection. Instead, the freshwater was forced through a narrow discharge "tube" at a higher velocity in between the upper saline plume and the underlying saltwater wedge, restricting the formation of fingering in this area and underscoring the complex nature of the onset of these events (Greskowiak 2014).

While density driven fingering has been studied in coastal areas using numerical modeling, the onset of density driven fingering events related to the dynamics of long term sea level rise within the setting of an island freshwater lens has yet to be explored. In this paper we examine the onset of density driven fingering in an island setting associated with groundwater inundation due to sea level rise. We used variable density groundwater flow and transport model, MODFLOW 6, to simulate a generalized island while varying key hydrogeologic parameters to understand the onset of density driven fingering and the impact it has on lake and groundwater salinity, as well as freshwater lens depletion.

4.2 Methods

We used MODFLOW 6 (Langevin et al. 2018), a variable density groundwater flow and transport model to generate 2D simulations of groundwater inundation caused by sea level rise for an idealized hypothetical island, similar to the methods used by Mancewicz et al. (2023). Only half of the island was represented in the domain due to symmetry. The domain consists of 500 columns and 130 layers with the top most layer at 4.65m elevation above sea level and the bottom at -80.35m. The grid cell size was finer in the upper portion of the domain from layer 0 to layer 89 (4.65m to -40.35m elevation) with grid cell dimensions of 0.5m tall by 1m wide. In the lower portion of the domain the cell dimensions were 1m by 1m. An area of lower elevation is located at left hand side of the domain (center of the island). Initially the water table is located below the bottom of this low lying area. As sea level rises, the water table intersects the low area and a lake begins to form. The bathymetry of the lake is that of a simplified "bucket" lake, with a flat bottom and vertical sides. The lake was represented using the Lake Package and Lake Transport Package.

A spin up simulation was used as the initial conditions for the transient sea level rise simulations and the timestep size was 1 day. A general head boundary condition with a constant concentration of 35 g/L was used on the vertical right hand side of the model domain to represent the ocean and a no flow boundary was assigned along the bottom and left side of the domain. The head for the general head boundary was kept fixed at an elevation of 0m for initial condition spin up simulations and was increased by a fixed increment each timestep for the SLR simulations. Viscosity was assumed constant and we used a homogeneous hydraulic conductivity of 10 m/d for the aquifer. A constant recharge rate of 20 cm/yr (0.00055 m/d) was used for all of the simulations. We used values for longitudinal and transverse dispersivity of 1 and 0.1, respectively and the

diffusivity was set to zero. This was done to allow us to concentrate on flow-driven phenomena.

We focused our sensitivity analysis on factors that were related to lake-groundwater dynamics and were thought to influence the formation of density gradients between the lake and underlying aquifer. A low (1m/100yrs or 2.73×10^{-5}m/d) and a high (2m/100yrs or 5.48×10^{-5}m/d) sea level rise rates were used. Lakebed sediments play an important role in governing lake-groundwater interactions and solute distribution patterns (Sheibani et al 2020). In MODFLOW 6, the parameter related to the lakebed sediments that is specified by the user is the lakebed leakage which is defined as:

$$L_{lake} = \frac{K_{lake}}{B_{lake}}$$

where L_{lake} is the lakebed leakage, K_{lake} is the hydraulic conductivity of the lakebed sediments and B_{lake} is the lakebed sediment thickness. For the Lake Package, the term that incorporates the lakebed leakage in calculating the flow between the lake and aquifer is the conductance (C_{lake}) which is defined as:

$$C_{lake} = \frac{A}{\left(\frac{1}{L_{lake}} + \frac{L}{K_{aquifer}}\right)}$$

assuming that the lakebed sediments and aquifer are connected in series where A is area perpendicular to flow, L is the distance between lakebed and aquifer cell node, and $K_{aquifer}$ is the hydraulic conductivity of the aquifer (Langevin et al. 2017). The lakebed leakage can be increased by either increasing the hydraulic conductivity of the lakebed sediments or by decreasing the thickness of the lakebed sediments. By increasing the lakebed leakage, the conductance increases and, keeping all other values constant, the flow between the lake and aquifer also increases. For our sensitivity analysis we used a base, low, and high lakebed leakage where the high lakebed leakage value results in a lakebed sediment conductance equal to the aquifer cell conductance (Table 2). Additionally, three different lake bottom widths (perpendicular to the coastline) were used (30m, 40m, and 60m). In total for the sensitivity analysis, we used three lake widths, two evaporation rates, three values for lakebed hydraulic conductivity, and two sea level rise rates (based on Sweet et al. 2017 for end of century sea level rise rates in the Caribbean), for a total of 36 transient sea level rise simulations. We refer to the scenario with a 30m wide lake, high evaporation rate, "base" lakebed conductance and high sea level rise rate as the base case. The base case is used to explain the overall phenomena, then we compare the base case to the results of the sensitivity analysis.

Table 1: Summary of simulation descriptions.

Name	Lake width	Lake evaporation	Lakebed hydraulic conductivity	SLR

S3-1	30	high	aquifer	low
S3-2	30	high	aquifer	high
S3-3	30	high	base	low
S3-4	30	high	base	high
S3-5	30	high	low	low
S3-6	30	high	low	high
S3-7	30	low	aquifer	low
S3-8	30	low	aquifer	high
S3-9	30	low	base	low
S3-10	30	low	base	high
S3-11	30	low	low	low
S3-12	30	low	low	high
S4-1	40	high	aquifer	low
S4-2	40	high	aquifer	high
S4-3	40	high	base	low
S4-4	40	high	base	high
S4-5	40	high	low	low
S4-6	40	high	low	high
S4-7	40	low	aquifer	low
S4-8	40	low	aquifer	high
S4-9	40	low	base	low
S4-10	40	low	base	high
S4-11	40	low	low	low
S4-12	40	low	low	high
S6-1	60	high	aquifer	low
S6-2	60	high	aquifer	high
S6-3	60	high	base	low
S6-4	60	high	base	high
S6-5	60	high	low	low
S6-6	60	high	low	high
S6-7	60	low	aquifer	low
S6-8	60	low	aquifer	high
S6-9	60	low	base	low
S6-10	60	low	base	high
S6-11	60	low	low	low
S6-12	60	low	low	high

Table 2: Values for descriptions used in defining simulation scenarios

Parameter	**Description**	**Value**	**Units**
Lake width	30	30	m
	40	40	m
	60	60	m

Lake evaporation	high	0.00165	m/d
	low	0.000825	m/d
Lakebed hydraulic conductivity	aquifer	10	m/d
	base	0.1	m/d
	low	0.01	m/d
SLR	low	1	m/100yr
	high	2	m/100yr

In order to make comparisons of the head gradient that governs flow between the lake and the aquifer, the values must first be converted to freshwater equivalent head. In the field, hydraulic head is measured as the height that groundwater rises within an observation well relative to sea level, which is a function of the groundwater density. The freshwater equivalent head is the height that the water in the piezometer would rise if it were filled with freshwater. By converting head to freshwater equivalent head, it allows head measurements with different densities to be more directly compared.

In analyzing the results from numerical simulations involving density driven fingering, dimensionless numbers have been used to quantify the onset of stability and classify flow regimes (Wooding, Tyler, and White 1997; Simmons, Narayan, and Wooding 1999; Greskowiak 2014; Schincariol, Schwartz, and Mendoza 1994; van Duijn, Pieters, and Raats 2019; Liu and Tokunaga 2020; Ketabchi et al. 2014; Habtemichael, Kiflemariam, and Fuentes 2014; Post and Houben 2017; Juster et al. 1997). Specifically relevant in these simulations is the mixed convection ratio (M). This nondimensional number was used by Liu and Tokunaga (2020) to identify certain regimes based off of fingering plume and flow behavior. The expression used here for the mixed convection ratio is defined as:

$$M = \frac{X_s}{\left(\frac{h_{lake} - h_{cell}}{\Delta z}\right)}$$

where h_{lake} and h_{cell} is the freshwater equivalent head in the lake and connection cell respectively, Δz is the distance between where h_{lake} and h_{cell} were calculated and

$$X_s = \frac{\rho_{avg} - \rho_f}{\rho_f}$$

where ρ_{avg} is the average density of the water in the lake and connection cell, and ρ_f is the density of freshwater. The numerator represents the total flux of density driven flow and the denominator represents total flux of hydraulically driven flow. For M >> 1, density driven processes are dominant and density driven fingering is expected to occur. In our simulations, the onset of a density driven fingering event was specified based on the response in lake concentration. The event was said to begin at the time step where the

lake concentration peaked before dropping during the event and was said to end the timestep that the concentration began to increase.

We also examined the effect of density driven fingering events on the freshwater lens. The extent of the freshwater lens refers to the total number of freshwater grid cells, which were defined as having a salinity less than 1.0 g/L. To compare the relative change in the size of the freshwater lens over time, the number of freshwater cells was normalized by the number of freshwater cells in the initial conditions, giving a percentage of the initial freshwater lens size for each timestep.

The following results section examines the lake salinity and DF event for S3-4 which is used as base case. Following, are the results of the sensitivity analysis which shows the impact of each parameter that was varied on six types of observations: lake salinity, freshwater lens depletion, when a DF does or doesn't occur, the magnitude of a DF event as specified by the amount of mass lost during the event, the timing of the DF event, and the mixed convection ratio. When referencing specific simulations, a shorthand version of the description is used in the results section. The parameters for a simulation are referenced in the following notation: (lake width / lakebed hydraulic conductivity (K) / SLR rate). For example, the shorthand notation for parameters associated with fr2hbab is (60m wide/base K/1m SLR).

4.3 Results

4.3.1 Base case – S3-4

4.3.1.1 Lake Salinity

For the base case, at the beginning of the sea level rise simulation the lake salinity remains close to 0 g/L. As sea level rises, the lake salinity begins to steadily increase, reaching a maximum of 4 g/L (Figure 1). The loss of water from evaporation drives the flow of water into the lake. During this period, all of the flow in the vertical direction is into the bottom of the lake (Figure 3) As sea level rises, the flow underneath the lake becomes more saline. The water flowing into the lake from the vertical direction contains more salt, which is added to the lake and increases the lake salinity. Additionally, freshwater is lost from the lake through evaporation, which concentrates the mass within the lake and increases lake salinity.

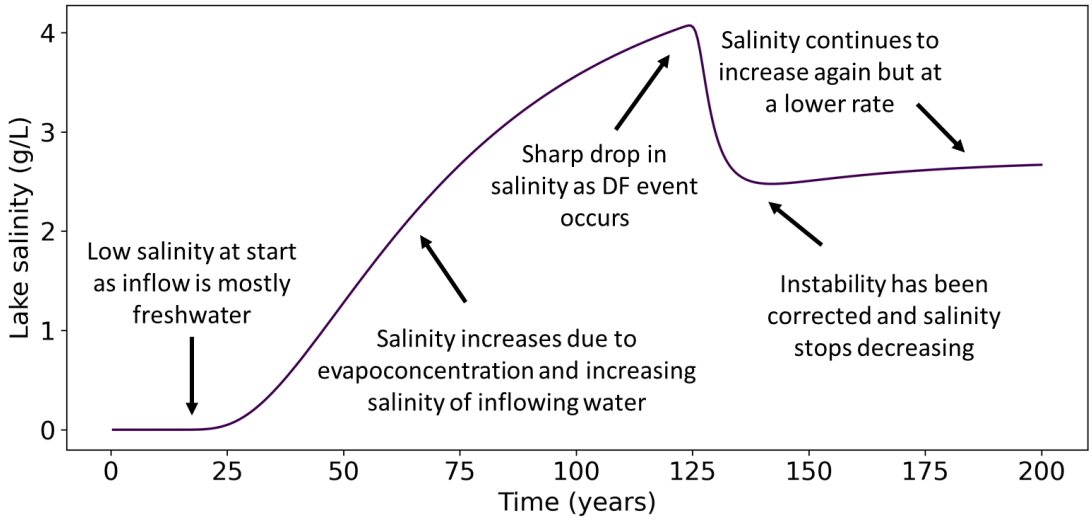

Figure 1: Lake salinity over time for base case simulation S3-4. The DF event occurs after 124 years into the simulation and is easily identified by the sharp drop in lake salinity. After the event, the salinity continues to increase but at a much lower rate.

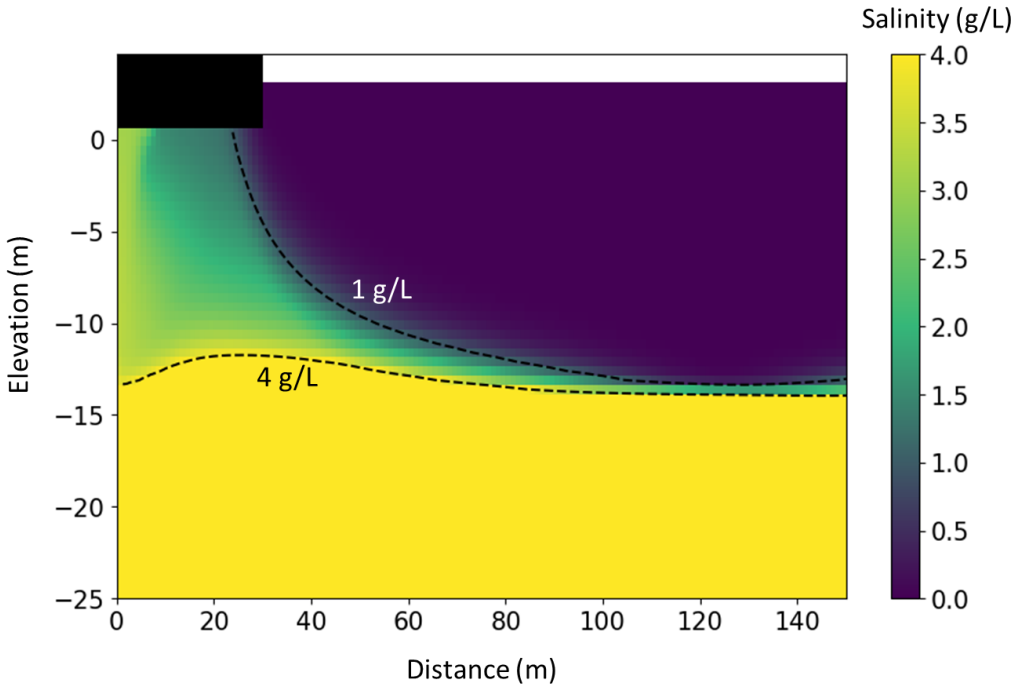

Figure 2: Cross section of groundwater salinity within the vicinity of the lake after 125 years of sea level rise for the base case simulation S3-4. The DF event can be seen on the left side of the lake bottom as a plume of higher salinity water from the lake intruding into the lower salinity groundwater. Also shown are the 1g/L and 4g/L contour lines.

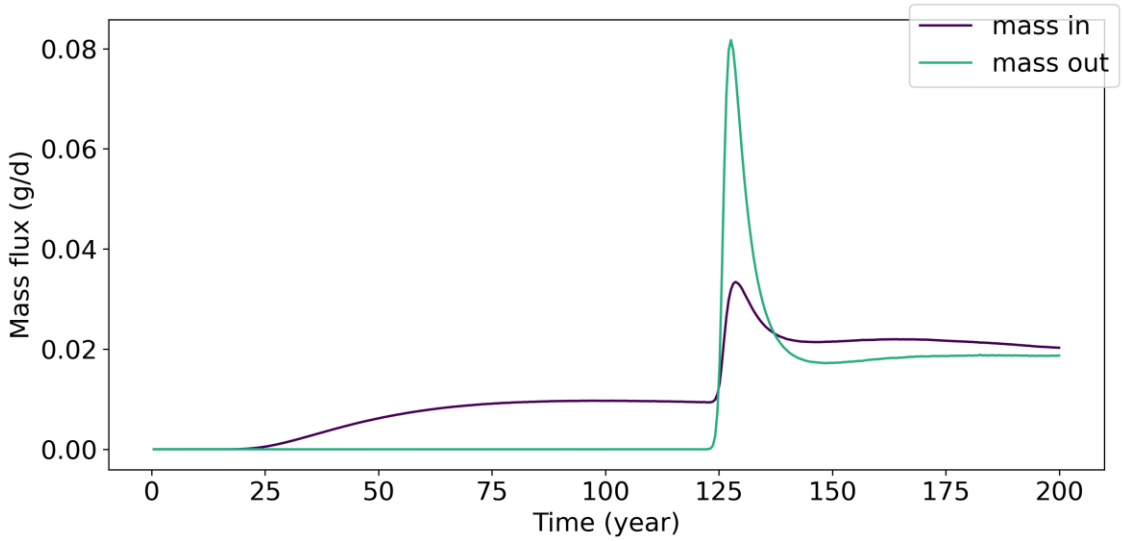

Figure 3: Mass flux of salt in and out for S3-4 along the lake bottom in the vertical direction. The DF event occurs after 124 years, where there is a sharp increase in the mass flux out of the lake. There is no mass flux out of the lake until after the DF event occurs.

At 124 years into the simulation, there is a drop in lake salinity to 2.5 g/L over a span of 18 years when the DF occurs as a plume of higher salinity lake water flows out of the bottom of the lake (Figure 2). The dynamics of the DF event are discussed in more detail in the next section. After the event, the lake salinity continues to steadily increase, but at a lower rate compared to before the DF event (Figure 3). Prior to the event, there is no loss of mass from the lake; all of the flow is into the lake, with the exception of evaporation which is only a freshwater loss. The area near where the event occurred along the lake bottom continues to act as an area of outflow where mass is lost from the lake into the underlying aquifer and the salinity of the lake increases at a lower rate than before the event.

4.3.1.2 DF event

At 124 years into the simulation, the DF event occurs on the left side of the lake over three connection cells (3m) (Figure 4). Leading up to the DF event, there is a small difference between the salinity, and consequently the density, of the lake and the groundwater as the area underneath the lake becomes increasingly brackish and the lake salinity increases. Once the water table inundates the low lying area and the lake turns on, the lake connection cells no longer directly receive freshwater recharge and the salinity of the aquifer underneath the lake increases. Additionally, as sea level rises, the freshwater lens also rises, putting the base of the lens closer to the lake bottom. The salinity of the lake is also increasing due to the inflow of mass from the aquifer and from evapoconcentration. The right side of the lake, however, remains fresh and there is a greater difference in density between the lake and the aquifer in this area. There is also less of a difference in total freshwater equivalent head between the lake and the aquifer

on the left side of the lake compared to the right side (Figure 4). This makes the left side of the lake more “vulnerable” for a potential DF event, should an instability develop.

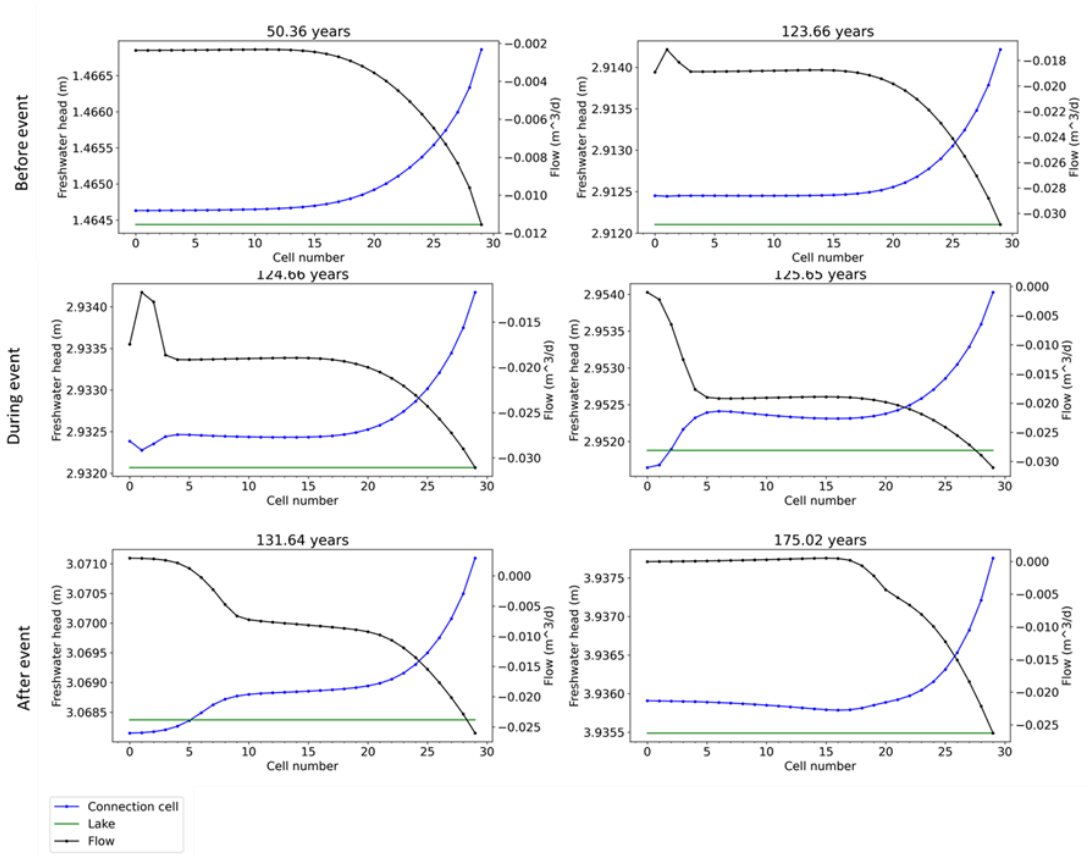

Figure 4: Changes to the equivalent freshwater head in the lake and connection cells and vertical flow in/out of the lake bottom. The lake and connection cell freshwater head are read on the left axis and the flow is read on the right. Each individual figure shows the flow and head across all lake connection cells for a single timestep where cell 0 is the leftmost edge of the lake and cell 30 is the right most edge. Positive values for flow indicate that flow is out of the lake into the connection cells. The timestep in years is displayed above each figure. Figures in the first, second, and third rows are from timesteps prior to the event, during the event, and after the event respectively.

At ~123 years into the simulation, the inflow from the vertical connection cells begins to decrease in the cells where the event occurs. The change in flow prior to the DF event is followed by a change in total equivalent freshwater head (Figure 4). This supports the idea that the DF is a density driven event because the change in head is not what initiates the response. Instead, the flow begins to change while the head remains constant. The flow in the area where the event occurs continues to decrease until becoming positive, indicating that flow is now going from the lake into the connection cells in this area along the lake bottom. Similarly, the equivalent freshwater total head in the connection cells on the left side of the lake continues to decrease at this time and is less than the equivalent

freshwater total head of the lake. The relative difference in head between the lake and aquifer is proportional to the magnitude of flow between the lake and aquifer.

After the DF event occurs, a new pattern forms in the head and flow distribution across the lake bottom (Figure 4). As the flow decreases on the left side of the lake, there is a corresponding drop in freshwater equivalent total head in the aquifer connection cells. Additionally on the left side of the lake, the flow out of the lake continues to decrease but there remains an area of outflow from the lake to the connection cells. The area where outflow occurs gradually extends further to the right side of the lake overtime. However, the direction of flow does not align with the relative difference in freshwater equivalent head between the lake and the aquifer. After the event, the freshwater equivalent total head in the connection cells begins to increase, until it is greater than the equivalent freshwater total head in the lake. If the direction of flow was governed by the difference in head alone, it would be expected in this case that flow would be from the aquifer (greater head) into the lake (lower head). However, the opposite occurs, suggesting that even after the DF event, density driven flow continues to govern the flow patterns between the lake and aquifer.

4.3.2 Sensitivity analysis

4.3.2.1 Lake Salinity

The lake salinity at the end of the simulation is greater with increasing lake width. The final lake salinity for the 30m wide lake where a DF event occurs ranges from 2.40 – 2.69 g/L. The final lake salinity for 40m wide lake ranges from 5.83 – 6.31 g/L and is on average 2.4x greater than the 30m wide lake. The final lake salinity for 60m wide lake ranges with low evaporation range from 2.38 – 3.01 g/L, while those with high evaporation range from 21.00 – 25.63 g/L and are on average 8.3x greater than the 30m wide lake. Over the span of a DF event, the percent difference in lake salinity from the start to the end of the even ranges from 7 – 85%. The drop in salinity during the DF event is greater with increasing lake width. For example, for S3-4 (30m wide/high evaporation/base K/high SLR) the percent difference in salinity from before to after the DF event is 39%, while for S6-4, which has the same properties as S3-4 except for a lake width of 60m, the percent difference is 61% (Table 3, Figure 5). Increasing the lake width by one third (from 30m to 40m) increases the change in salinity from the start to the end of the DF event by a factor of 1.2 for high SLR and 1.1 for low SLR. By doubling the lake width (from 30m to 60m), the change in salinity from the start of the DF event to the end of the DF event increases by a factor of 1.5 for the high SLR rate and 1.2 for the low SLR rate. When the water table rises above the land surface the water floods the low-lying depression and forms a lake. When this occurs within MODFLOW 6 the Lake Package is “turned on” and aquifer cells designated as lake connection cells no longer receive land surface recharge. The reduction in freshwater recharge contributes to increasing salinity underneath the lake. The greater the lake width, the more lake connection cells turn on and the greater the reduction in recharge.

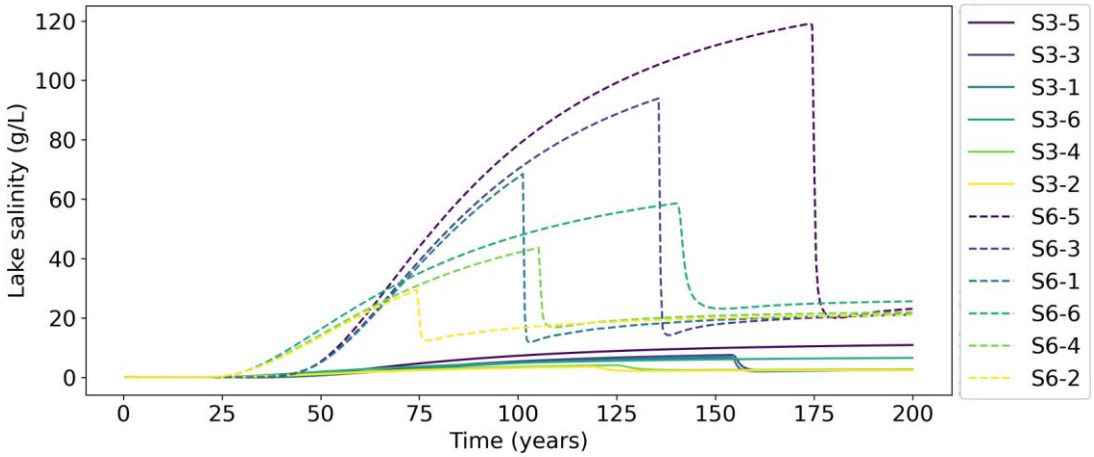

Figure 5: The lake salinity over time for selected simulations from the sensitivity analysis. The group of simulations includes (30 and 60m / high evaporation / aquifer, base and low K / low and high SLR). The solid curve shows the results for the 30m wide lake simulations, and the dashed line shows the results for the 60m wide lake simulations.

Table 3: Lake salinity at the end of the simulation, the maximum lake salinity that occurred during the simulation and the change in the freshwater lens from the initial conditions to the final timestep for all simulations

Name	**Final lake salinity (g/L)**	**Max lake salinity (g/L)**	**Percent difference in the number of freshwater cells (%)**
S3-1	2.46	6.80	67.28
S3-2	2.40	3.57	56.81
S3-3	2.69	7.56	67.48
S3-4	2.67	4.07	57.19
S3-5	10.90	10.90	71.42
S3-6	6.58	6.58	59.41
S3-7	0.37	0.37	80.45
S3-8	0.24	0.24	68.42
S3-9	0.47	0.47	80.48
S3-10	0.30	0.30	68.62
S3-11	0.83	0.83	80.35
S3-12	0.56	0.56	68.28
S4-1	5.95	18.41	59.22
S4-2	5.83	9.45	48.96
S4-3	6.31	20.43	59.15
S4-4	6.28	10.67	49.25
S4-5	28.00	28.00	63.22
S4-6	16.30	16.30	51.63

S4-7	1.05	1.05	75.66
S4-8	0.64	0.64	63.47
S4-9	1.22	1.22	75.50
S4-10	0.77	0.77	63.59
S4-11	1.90	1.90	75.23
S4-12	1.27	1.27	62.81
S6-1	21.19	68.52	43.48
S6-2	21.00	29.48	33.50
S6-3	21.10	93.95	44.09
S6-4	21.86	43.65	33.70
S6-5	23.09	119.14	43.09
S6-6	25.63	58.60	34.58
S6-7	2.42	4.42	57.72
S6-8	2.38	2.47	47.50
S6-9	3.02	5.03	58.46
S6-10	2.69	2.82	48.01
S6-11	6.63	6.63	60.05
S6-12	4.38	4.38	49.08

While simulations with high evaporation that have a DF event reach salinities greater than 100 g/L, simulations with low evaporation do not exceed 3.0 g/L (Table 3, Figure 5). There were only four simulations with low evaporation that also had a DF event occur so direct comparison between the high and low evaporation rate was only done for the 60m wide simulations with a base or aquifer lakebed hydraulic conductivity and for high and low SLR. For this set of simulations, the ones with the high evaporation rate had a final lake salinity ~8 times greater than simulations with a low evaporation rate. Evaporation not only increases lake salinity through evapoconcentration of the solutes within the lake, but also drives upconing of higher salinity water underneath the lake. This means that the salinity of the inflowing water from the aquifer into the lake is also increasing and contributes to overall greater lake salinity. Similarly, there is a greater change in lake salinity over the course of the DF event for the high evaporation simulations. For the high evaporation rate, the percent difference in lake salinity over the duration of the event ranges from 48 – 85%. For the low evaporation rate, the percent difference in lake salinity over the duration of the event ranges from 7 – 47%. For the low evaporation rate, there is less of an effect from evapoconcentration and upconing on the lake salinity. There is less of a difference in salinity between the lake and the underlying groundwater and less of an instability to alleviate through a DF event so the change in salinity over the course of the event is smaller for the low evaporation simulations compared to the high evaporation.

The percent difference in lake salinity from the start to the end of the event is consistent across lakebed hydraulic conductivities and this parameter is not a key factor in determining the decrease in lake salinity over the course of the DF event (Figure 5).

However, the final lake salinity at the end of a simulation does vary with lakebed hydraulic conductivity and is greatest for low lakebed hydraulic conductivity. The low lakebed hydraulic conductivity isolates the lake from the groundwater allowing the salinity to increase through evapotranspiration while inhibiting or delaying a DF event. For example, the flow into and out of the lake bottom is an order of magnitude lower for S6-5 (60m wide/high evaporation/low K/1m SLR) compared to S6-3 (60m wide/base K/1m SLR) and the lake salinity for S6-5 reaches 119 g/L before an event occurs (Figure 5).

The SLR rate impacts the change in lake salinity over the duration of the event, but the overall final lake salinity at the end of the simulation for the high and low SLR rate simulations generally differ by <1 g/L (Figure 4). For low SLR rate, the percent difference in the lake salinity over the duration of the event is greater than for the high SLR rate. Doubling the sea level rise rate results in 30% less decrease in lake salinity over the course of the event. For example, for S3-3 (30m wide/high evaporation/base K/1m SLR) the percent difference in lake salinity over the duration of the event is 70%, while for S3-4 (30m wide/high evaporation/base K/2m SLR) the percent difference is 39% and the two values differ by a value of 31% (Figure 5, Table 3). The change in lake salinity over the event is not only a function of the loss of higher salinity water out of the lake, but is also dependent on the corresponding influx of water into the lake. For the low SLR rate, the freshwater lens does not salinize as quickly and the inflowing water within the vicinity of the lake is not as saline as for the high SLR rate simulations.

4.3.2.2 Freshwater lens depletion

The DF event causes a 2 – 12% drop in the number of freshwater cells over the duration of the event (Table 3). The simulations that have approximately a 2% drop in the extent of the freshwater lens over the duration of the event all have high evaporation, high aquifer lakebed hydraulic conductivity, include both the low and high SLR rate and are either 40m or 60m wide. Because of the higher lakebed hydraulic conductivity, there is greater flow between the lake and aquifer and advection of mass into the lake. The wider the lake, the greater the width over which this occurs. Consequently, the salinity of the groundwater within the vicinity of the lake is more similar to the salinity of the lake so that when the event occurs, there is not as much of a change in the number of freshwater cells. The greatest drop in freshwater lens extent over the duration of the event occurs for the 60m wide, high evaporation, low lakebed hydraulic conductivity scenarios (Figure 6). For these simulations, the underlying aquifer is more isolated from the lake due to the low lakebed hydraulic conductivity which inhibits a DF event from occurring. The high evaporation rate causes evapoconcentration of solutes within the lake, increasing the lake salinity. When the event does occur, much higher salinity water disperses into the underlying area, decreasing the overall number of freshwater cells within the vicinity of the lake. In general, outside of these two extreme cases, there is little difference in the change to the extent of the freshwater lens over the duration of the event between the different scenarios. There is <1% change in the extent of the freshwater lens over the course of the event when just comparing across SLR rate or lakebed hydraulic

conductivity and <3% change in the extent of the freshwater lens when comparing lake width or evaporation rate, keeping all other parameters the same.

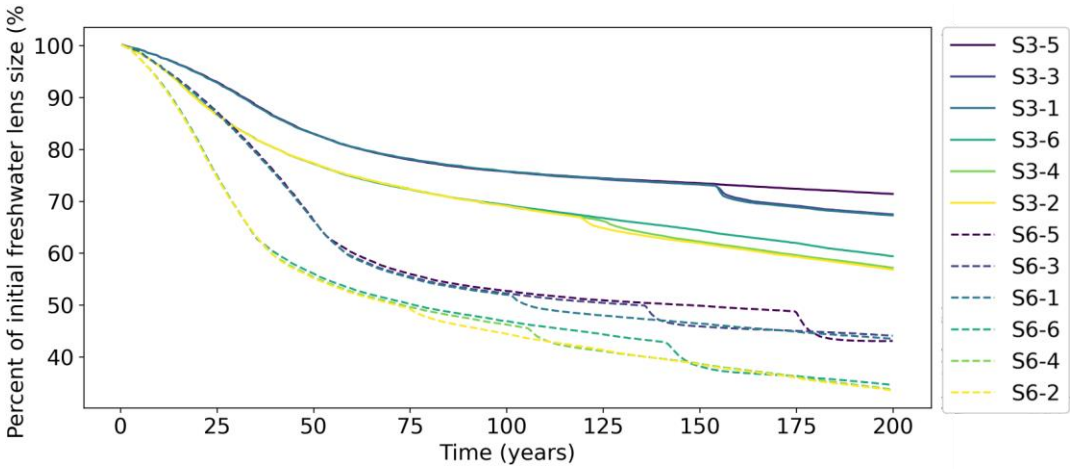

Figure 6: The change in the extent of the freshwater lens over time relative to the initial conditions. The simulations shown here are the same as in Figure 4. The group of simulations includes (30 and 60m / high evaporation / aquifer, base and low K / low and high SLR). The solid curve shows the results for the 30m wide lake simulations, and the dashed line shows the results for the 30m wide lake simulations. The impact of the DF event is clearly seen as the sudden decrease in freshwater lens size.

The final extent of the freshwater lens is greater for simulations with high evaporation rate compared to the low evaporation rate. This effect scales with lake width (Figure 6). When the lake width is doubled, the percent difference in the extent of the freshwater lens between high and low evaporation rate also increases by a factor of approximately two. This suggests that as the lake width increases, the lake evaporation rate plays a stronger role in the final extent of the freshwater lens. A wider lake leads to greater surface area for evaporation and also a greater area of upconing of higher salinity groundwater underneath the lake, resulting in greater freshwater loss.

Simulations have similar long-term freshwater lens depletion trends for a given set of properties, regardless of the lakebed conductance (Figure 5). For simulations with a DF event, the event realigns the trajectory of freshwater lens depletion with the other simulations in that set. Overall, the average percent difference in the final extent of the freshwater lens for the low and aquifer lakebed K scenarios compared to the base case across all simulations is ~2%.

After an initial response and adjustment period where the low-lying area becomes flooded and the lake “turns on”, the freshwater lens depletion becomes linear and is parallel amongst simulations that have the same SLR rate. As sea level rises, the freshwater lens also rises, and the number of freshwater cells decreases. The head for the general head boundary condition used to represent sea level was increased by a fixed amount each timestep so it would be expected that the freshwater lens depletion would

also be linear, with the exception of the DF events. Doubling the SLR rate from 1m/100yrs to 2m/100yrs increases the freshwater loss at the end of the simulation by 15%, keeping all other parameters the same, regardless of whether or not a DF event occurs.

4.3.2.3 DF event occurrence

There are certain sets of scenarios where a DF event consistently either occurred or did not occur regardless of changes to other properties (Table 4) over the duration of our simulations. For scenarios with low evaporation and low lakebed K, no DF event occurs, regardless of lake width or SLR rate. A low lakebed hydraulic conductivity isolates the lake from the aquifer and limits the exchange of water between the lake and aquifer. Additionally, the low evaporation rate means that less fresh water is lost from the lake, resulting in fresher lake salinities and less of a difference in density between the lake and aquifer. For scenarios with a high evaporation rate and either the base lakebed hydraulic conductivity or aquifer hydraulic conductivity, regardless of the lake width or sea level rise rate, a DF event occurred. This is due to the high evaporation rate, which increases the lake salinity by evapoconcentration.

Table 4: Results for simulations where a DF event occurs for before and after the event

Name	**Start of DF event (yr)**	**End of DF event (yr)**	**Lake salinity at start of DF event (g/L)**	**Lake salinity at end of DF event (g/L)**	**Mass out of lake during DF event (g)**	**M at start of DF event**	**M at end of DF event**
S3-1	154.08	162.05	6.80	1.99	1.62	5.64	0.45
S3-2	118.67	132.14	3.57	2.16	1.14	4.67	0.45
S3-3	154.08	164.55	7.56	2.28	1.76	4.74	0.48
S3-4	124.16	142.11	4.07	2.48	1.36	3.81	0.49
S4-1	135.13	139.12	18.41	4.36	5.04	5.99	0.47
S4-2	105.71	111.19	9.45	4.82	3.65	5.10	0.51
S4-3	143.61	149.59	20.43	4.83	5.53	5.58	0.47
S4-4	114.68	124.66	10.67	5.51	4.39	4.80	0.53
S6-1	101.22	103.22	68.52	11.84	10.64	5.88	0.88
S6-2	74.30	77.29	29.48	12.39	13.20	5.21	0.82
S6-3	135.63	138.12	93.95	14.20	32.67	6.16	0.23
S6-4	105.21	109.20	43.65	16.88	26.03	5.75	0.36
S6-5	174.02	181.00	119.14	20.04	50.73	5.46	0.50
S6-6	140.12	152.08	58.60	23.13	46.86	4.96	0.39
S6-7	176.02	187.48	4.42	2.33	2.10	4.83	0.80
S6-8	134.13	148.59	2.47	2.21	0.91	3.04	0.98
S6-9	193.47	199.45	5.03	3.09	1.59	4.47	1.23
S6-10	147.10	171.53	2.82	2.63	0.93	2.62	0.89

The wider the lake the more likely it is for DF to occur within our simulations. A DF event occurs for all but two cases for the widest lake (60m wide), regardless of other lake properties or SLR rate. The wider the lake, the more lake connection cells there are that get "turned on" and the greater the reduction in land surface recharge affecting lake and groundwater salinity. Additionally, the wider the lake the greater the area of evaporation driven upconing underneath the lake, which also impacts lake and aquifer salinity.

In most cases, the low evaporation rate is not high enough to drive increasing lake salinity through evapoconcentration that produces a great enough density gradient between the lake and underlying groundwater to cause a DF event. Instead, for most cases the high evaporation rate is required to drive evapoconcentration within the lake and increase the lake salinity enough to create a sufficient density difference between the lake and the aquifer for a DF event to occur.

For the aquifer and base lakebed hydraulic conductivity, the determining factor in whether or not a DF event occurs is the evaporation rate, not the lakebed hydraulic itself; a DF event only occurs for the high evaporation rate simulations. There are only four simulations with a low lakebed hydraulic conductivity where there is also a DF event. In general, the low lakebed hydraulic conductivity isolates the lake from the aquifer and inhibits the formation of a DF event.

For a particular set of properties, varying the SLR rate alone does not change whether or not a DF event occurs. For example, there is no DF event for the 30m wide high evaporation low lakebed hydraulic conductivity scenarios with either the high or low SLR rate (S3-5 or S3-6). Overall, the lake characteristics are more important than SLR rate alone when it comes to determining whether or not a DF event will occur.

4.3.2.4 Mass lost during a DF event

The amount of mass lost during an event is a function of the difference in density between the lake and aquifer. In general, the greater the difference in density between the lake and the underlying aquifer, the more mass is lost from the lake during the DF event in order to correct the instability. The mass lost over the duration of the event increases with increasing lake width (Table 4). Increasing the lake width by around one third (from 30m to 40m) increases the amount of mass lost from the lake by a factor of ~3. However, doubling the lake width from 30m to 60m increase the mass lost by a factor of 7 – 19, depending on the lake hydraulic conductivity and the SLR rate. The amount of mass lost from the lake is proportional to changes in lake width at smaller lake widths by a fixed factor regardless of other parameters, but for larger lake widths the relationship depends on additional factors.

The mass lost during the DF event is greater for the high evaporation rate scenarios compared to those with a low evaporation rate. The high evaporation scenarios ranged from 5 – 28 times greater mass lost than the low evaporation rate scenarios, keeping other properties the same. This large range in the difference between the low and high evaporation scenarios is secondarily a function of lakebed hydraulic conductivity and

SLR rate. This shows the importance of other factors in determining the amount of mass lost during the DF event rather than evaporation alone.

As the lakebed hydraulic conductivity increases, the amount of mass lost during the DF event decreases (Table 4). There is less mass out during the DF event for the scenarios with the aquifer lakebed hydraulic conductivity because there is greater flow, and consequently greater mass, exchanged between the lake and the aquifer through advection. Because of this ongoing advection, the change in mass that occurs during the event is not as much compared to the simulations with a lower lakebed hydraulic conductivity. There is greater mass lost from the lake into the aquifer during the DF event for the low lakebed hydraulic conductivity because the low hydraulic conductivity inhibits the DF event from occurring and evaporation rate continues to increase. When the DF event does eventually occur, the lake is at a much greater salinity compared to other simulations with similar properties, and more mass is lost from the lake during the event to correct the instability caused by the difference in density between the lake and the aquifer.

There is a greater loss of mass out of the lake during the DF event for the low SLR rate compared to the high SLR rate. For the low SLR rate simulations, the base of the freshwater lens rises more slowly and the area underneath the lake takes longer to salinize. However, the lake continues to increase in salinity through evapoconcentration and leads to a greater difference in salinity between the slowly salinizing freshwater lens and the evapoconcentrating lake. This results in a greater salinity difference between the lake and the aquifer, and more mass is lost from the lake to resolve the instability compared to the high SLR simulations.

4.3.2.5 Timing of DF events

As lake width increases, the DF event occurs sooner (Table 3, Figure 5). If the lake width is doubled (from 30m to 60m) the DF event occurs 18-53 years sooner. If the lake width is increased by about one third (from 30m to 40m) the event occurs 10-19 years sooner. For the wider lake simulations, effects of upconing and evapoconcentration occur more rapidly than for the narrower lake simulations. These broad ranges in event onset are secondarily a function of lakebed hydraulic conductivity. For example, the difference between the 60m wide and 30m wide lake with the aquifer hydraulic conductivity range from 44 – 53 years, while the difference between the 60 and 30m wide lake with the base hydraulic conductivity was 19 years. Therefore, lakebed width alone is not a determining factor in determining the onset of the DF event.

For the high evaporation rate scenarios, the DF event occurs 42 – 75 years sooner than for the low evaporation rate simulations (Table 4). For simulations with the high evaporation rate, the difference in density between the lake and underlying groundwater is established more quickly due to the effects of evaporation on evapoconcentration. The DF event occurs later for scenarios with a lower value for lakebed hydraulic conductivity compared to those with a higher lakebed hydraulic conductivity. The low lakebed hydraulic conductivity isolates the lake from the aquifer and delays the onset of the DF event.

The event for the high SLR rate simulations occurs between 27 – 46 years later than for the low SLR rate simulations, with an average difference of 34 years (Table 4). The DF event for the high SLR simulations occurs later because as the lake salinity is increasing due to evapoconcentration, the groundwater salinity under the lake is also increasing more quickly than the low SLR scenario as the freshwater lens "floats" upwards. Since the groundwater salinity is increasing more so compared to the low SLR case, there is less of a difference in salinity between the lake and the aquifer until later in the simulation once the lake salinity has increased enough to cause a DF event.

4.3.2.6 Mixed convection ratio

The average value for M across all lake connection cells along the lake bottom is <6.16 at the start of a DF event for all scenarios where an event occurs. For most simulations, M increases until reaching a value of approximately 5 before an event occurs. The results are similar regardless of parameters used and a value of 5 appears to be a cutoff value for the onset of a DF. The value of M at the end of the event is <1 for all simulations, which indicates that the instability has been corrected.

4.4 Discussion

A DF event is driven by the difference in density between the lake and the underlying aquifer. From our results there are five key processes that control the onset, duration and magnitude of a DF event and the effect on lake salinity and the extent of the freshwater lens. This includes (1) changes in land surface recharge, (2) upconing, (3) evapoconcentration, (4) upward movement of the freshwater lens from SLR, and (5) connection/isolation between the lake and aquifer. When the lake "turns on" the lake connection cells no longer receive fresh land surface recharge contributing to an increase in salinity in the area underneath the lake. Upconing occurs underneath the lake as freshwater is drawn upwards to meet the evaporative demand of the lake and contributes to increasing salinity underneath the lake. Evapoconcentration occurs within the lake as freshwater evaporates from the lake, leaving the solutes to accumulate within the lake and increasing the lake salinity. As sea level rises, the base of the freshwater lens also rises and the overall salinity of the aquifer increases. The hydraulic connection between the lake and the aquifer influences advection and the accumulation of solutes within the lake.

If we consider the 2D domain to exist in the x and z planes where the lake has some width and depth, then for a 3D simulation the length of the lake would exist in the y plane. For the 2D simulations, when the lake "turns on" the aquifer cells no longer receive land surface recharge and salinization occurs within the vicinity of the lake. In a 3D case, the lateral ends of the lake in the y direction would be closer to areas still receiving freshwater recharge. This could have the effect of decreasing the salinization of the groundwater in the area near the lake ends and increasing the difference in salinity between the lake and the average connection cell density.

When a DF event occurs, there is a sudden drop in the extent of the freshwater lens. In terms of water management, while there is a drop in the freshwater lens, the impact to the

overall lens is limited to the vicinity of the lake. Additionally, the DF event occurs over a span of several years, so any impact is not immediately a threat to freshwater availability.

While we present conclusions relevant to the onset of DF events, our results are not meant to be predictive of specific events. Instead, they are meant to explore the general relationship between different hydrogeologic settings and the impact of a DF event on lake salinity and the extent of the freshwater lens. Additionally, our results are partly a function of the discretization that was used. For example, a DF event on a grid with finer spatial discretization could have a more distinct shape/boundary compared to a coarser discretization. Since the impact to the freshwater lens was assessed by counting individual cells with a certain concentration, using a finer grid could result in a slightly different impact to the freshwater lens extent. Furthermore, there were certain simulations where DF events do not occur for the parameters used in our simulations. However, it is likely that if the simulations were continued to run, at some point in the future a DF event would eventually occur.

There were also simplifications made to the conceptual model in order to examine the hydrodynamics of groundwater inundation and DF events at a fundamental level. This includes simplifying the geometry of the lake to a "bucket" shape and excluding coastal inundation. Seasonal and tidal variation was also not included in our simulations. It is expected that if additional mixing from seasonal or tidal effects was included, it would enhance further loss of the freshwater land and contribute to increasing lake salinity. We also do not consider the impacts of precipitation and dissolution of solutes within the lake. In the lakes on San Salvador Island, as salinity increases salts can precipitate out of solution, reducing the overall lake salinity. These salts may become buried or dissolve back into solution and further complicate the application of these results to the onset of DF events.

Future work could include further exploring the conditions under which a lake becomes hypersaline and the role that DF events could play in preventing hypersalinity from occurring. Additionally, the mixed convection ratio was used here to investigate the onset of a DF event. Another useful non-dimensional number is the Rayliegh number which relates the density driven forces to mixing related forces that inhibit the formation of DF events. These results could also be investigated within the context of the Rayliegh number to provide further insight to the behavior of DF events. Also, for several parameters considered, the narrower lakes behaved similarly, while the widest lake had unique results. As such, future work could also include investigating a wider range of lake widths greater than what was used here, to further evaluate the impact of lake width on the onset of DF events and the impact to lake salinity.

4.5 Conclusion

When a fluid of greater density overlies a fluid of lower density, a density driven plume, or finger, of the higher salinity water can intrude into the less dense underlying fluid, called a density driven fingering event. We explored DF events associated with SLR driven groundwater inundation on islands. We performed a sensitivity analysis to

determine what role certain hydrogeologic factors play in the impact of DF events on lake salinity and the freshwater lens. Five key processes were identified that contribute to the onset of DF events and the impact of DF events on the freshwater lens and lake salinity including: (1) changes in land surface recharge, (2) upconing, (3) evapoconcentration, (4) upward movement of the freshwater lens from SLR, and (5) connection/isolation between the lake and aquifer.

5 Chapter 5: Conclusion

Groundwater inundation due to sea level rise can have a negative impact on island freshwater supplies by exposing the water table to evaporative losses. In order to study the impact of groundwater inundation on the freshwater lens, we used the Lake Transport Package with MODFLOW 6, a variable density groundwater flow and transport model. Using the Lake Transport Package, we are able to represent the process of groundwater inundation due to sea level rise in a more effective way than past modeling efforts.

We applied this approach to investigate groundwater inundation due to sea level rise for a hydrogeologic setting that is commonly encountered on small islands; a lower layer of high hydraulic conductivity overlain by an upper low hydraulic conductivity layer. We performed a sensitivity analysis to explore if including these layers in our model setup made a significant difference in the extent of the freshwater lens and lake salinity compared to a simple homogeneous scenario. Ultimately, the initial conditions were the controlling factor in the difference between the homogeneous and two-layer scenarios, not specifically any processes directly related to sea level rise.

We also performed a sensitivity analysis to explore the impacts of density driven fingering events on the freshwater lens and lake salinity. These events arise when a more dense fluid overlays a less dense fluid, causing a plume, or finger, of the more dense fluid to intrude into the less dense fluid. This situation can occur due to groundwater inundation, as the newly formed lake undergoes evapoconcentration and increases in salinity. Five key processes were identified that contribute to the onset of DF events and the impact of DF events on the freshwater lens and lake salinity including: (1) changes in land surface recharge, (2) upconing, (3) evapoconcentration, (4) upward movement of the freshwater lens from SLR, and (5) connection/isolation between the lake and aquifer.

6 Works cited

Alsaffar, Abdul Kareem K., Riyadth Hamed, and Zaid H. Majeed. 2023. “A Comprehensive Analysis of Groundwater Inundation Vulnerability and Remediation for Infrastructures.” In *E3S Web of Conferences*. Vol. 427. EDP Sciences. https://doi.org/10.1051/e3sconf/202342704004.

Ayers, Jerry F., and H. L. Vacher. 1986. “Hydrogeology of an Atoll Island: A Conceptual Model from Detailed Study of a Micronesian Example.” *Groundwater* 24 (2): 185–98. https://doi.org/10.1111/j.1745-6584.1986.tb00994.x.

Bailey, R. T., J. W. Jenson, and A. E. Olsen. 2009. “Numerical Modeling of Atoll Island Hydrogeology.” *Ground Water* 47 (2): 184–96. https://doi.org/10.1111/j.1745-6584.2008.00520.x.

Bakker, Mark, Vincent Post, C. D. Langevin, J. D. Hughes, J. T. White, A. T. Leaf, S. R. Paulinski, et al. 2021. “FloPy.” U.S. Geological Survey Software Release. http://dx.doi.org/10.5066/F7BK19FH.

Bjerklie, David M., John R. Mullaney, Janet R. Stone, Brian J. Skinner, and Matthew A. Ramlow. 2012. “Simulations of the Effects of Sea-Level Rise on Groundwater Levels, New Haven, Connecticut.” *U.S. Geological Survey Open-File Report 2012-1025*.

Breithaupt, Charles I., Jason D. Gulley, Paul J. Moore, Shawn M. Fullmer, Charles Kerans, and Jessica Z. Mejia. 2021. “Flank Margin Caves Can Connect to Regionally Extensive Touching Vug Networks before Burial: Implications for Cave Formation and Fluid Flow.” *Earth Surface Processes and Landforms* 46 (8): 1458–81. https://doi.org/10.1002/esp.5114.

Cant, Richard V., and Philip S. Weech. 1986. “A Review of the Factors Affecting the Development of Ghyben-Hertzberg Lenses in the Bahamas.” *Journal of Hydrology* 84 (3): 333–43. https://doi.org/10.1016/0022-1694(86)90131-9.

Chambers, Lee A., Brioch Hemmings, Simon C. Cox, Catherine Moore, Matthew J. Knowling, Kevin Hayley, Jens Rekker, Frédérique M. Mourot, Phil Glassey, and Richard Levy. 2023. “Quantifying Uncertainty in the Temporal Disposition of Groundwater Inundation under Sea Level Rise Projections.” *Frontiers in Earth Science* 11. https://doi.org/10.3389/feart.2023.1111065.

Cheng, Xizngxue, and Mary P Anderson. 1993. “Numerical Simulation of Ground-Water Interaction with Lakes Allowing for Fluctuating Lake Levels.” *Ground Water* 31 (6): 929–33.

Cooper, Hannah M., Caiyun Zhang, and Donna Selch. 2015. “Incorporating Uncertainty of Groundwater Modeling in Sea-Level Rise Assessment: A Case Study in South Florida.” *Climatic Change* 129 (1–2): 281–94. https://doi.org/10.1007/s10584-015-

1334-1.

Council, Gregory W. 1997. “Simulating Lake-Groundwater Interaction with MODFLOW.” In *Proceedings of the 1997 Georgia Water Resources Conference*, 457–62. Athens, Georgia. https://smartech.gatech.edu/handle/1853/44196.

Diersch, H. J.G., and O. Kolditz. 2002. “Variable-Density Flow and Transport in Porous Media: Approaches and Challenges.” *Advances in Water Resources* 25 (8–12): 899–944. https://doi.org/10.1016/S0309-1708(02)00063-5.

Dose, Eduardo J., Leonard Stoeckl, Georg J. Houben, H. L. Vacher, Sara Vassolo, Jörg Dietrich, and Thomas Himmelsbach. 2014. “Experiments and Modeling of Freshwater Lenses in Layered Aquifers: Steady State Interface Geometry.” *Journal of Hydrology* 509: 621–30. https://doi.org/10.1016/j.jhydrol.2013.10.010.

Duijn, C. J. van, G. J.M. Pieters, and P. A.C. Raats. 2019. “On the Stability of Density Stratified Flow Below a Ponded Surface.” *Transport in Porous Media* 127 (3): 507–48. https://doi.org/10.1007/s11242-018-1209-9.

Duvat, Virginie K.E. 2019. “A Global Assessment of Atoll Island Planform Changes over the Past Decades.” *Wiley Interdisciplinary Reviews: Climate Change* 10 (1). https://doi.org/10.1002/wcc.557.

Ghyben, W.B. 1889. “Nota in Verband Met de Voorgenomen Putboring Nabij Amsterdam (Notes on the Probable Results of the Proposed Well Drilling near Amsterdam).” *Tijdschrift Het Koninklijk Instituut Voor Ingenieurs, The Hague*, 8–22.

Greskowiak, Janek. 2014. “Tide-Induced Salt-Fingering Flow during Submarine Groundwater Discharge.” *Geophysical Research Letters* 41 (18): 6413–19. https://doi.org/10.1002/2014GL061184.

Griggs, John E, and Frank L Peterson. n.d. “Ground-Water Flow Dynamics and Development Strategies at the Atoll Scale.”

Gulley, J. D., A. S. Mayer, J. B. Martin, and V. Bedekar. 2016. “Sea Level Rise and Inundation of Island Interiors: Assessing Impacts of Lake Formation and Evaporation on Water Resources in Arid Climates.” *Geophysical Research Letters* 43 (18): 9712–19. https://doi.org/10.1002/2016GL070667.

Guo, Weixing, and Christian D. Langevin. 2002. *User’s Guide to SEAWAT: A Computer Program for Simulation of Three-Dimensional Variable-Density Ground-Water Flow*. *USGS Techniques of Water Resources Investigations*.

Habel, Shellie, Charles H. Fletcher, Kolja Rotzoll, and Aly I. El-Kadi. 2017. “Development of a Model to Simulate Groundwater Inundation Induced by Sea-Level Rise and High Tides in Honolulu, Hawaii.” *Water Research* 114: 122–34.

https://doi.org/10.1016/j.watres.2017.02.035.

Habtemichael, Y.T., R.T. Kiflemariam, and H.R. Fuentes. 2014. “Evaluation of Instability of a Low-Salinity Density-Dependent Flow in a Porous Medium.” In *COMSOL Conference*. Boston. http://ovidsp.ovid.com/ovidweb.cgi?T=JS&PAGE=reference&D=emed11&NEWS=N&AN=70983170.

Herzberg, A. 1901. “Die Wasserversorgung Einiger Nordseebäder [The Water Supply of Some North Sea Spas].” *J Gasbeleucht Wasserversorg* XLIV (44): 815–19, 842–44.

Hoover, Daniel J., Kingsley O. Odigie, Peter W. Swarzenski, and Patrick Barnard. 2017. “Sea-Level Rise and Coastal Groundwater Inundation and Shoaling at Select Sites in California, USA.” *Journal of Hydrology: Regional Studies* 11: 234–49. https://doi.org/10.1016/j.ejrh.2015.12.055.

Hughes, J.D., C.D. Langevin, and E.R Banta. 2017. “Documentation for the MODFLOW 6 Framework.” *USGS: Techniques and Methods 6-A57*, 42.

Hunt, R J, H M Haitjema, J T Krohelski, and D T Feinstein. 2003. “Simulating Ground Water-Lake Interactions: Approaches and Insights: Invited Contribution for Special MODFLOW2001 Issue.” *Ground Water*.

Juster, Thomas, P. A. Kramer, H. L. Vacher, P. K. Swart, and M. Stewart. 1997. “Groundwater Flow beneath a Hypersaline Pond, Cluett Key, Florida Bay, Florida.” *Journal of Hydrology* 197 (1–4): 339–69. https://doi.org/10.1016/S0022-1694(96)03103-4.

Ketabchi, Hamed, Davood Mahmoodzadeh, Behzad Ataie-Ashtiani, Adrian D. Werner, and Craig T. Simmons. 2014. “Sea-Level Rise Impact on Fresh Groundwater Lenses in Two-Layer Small Islands.” *Hydrological Processes* 28 (24): 5938–53. https://doi.org/10.1002/hyp.10059.

Konikow, L.F, D.J. Goode, and G.Z. Hornberger. 1996. “A Three-Dimensional Method-of-Characteristics Solute- Transport Model (MOC3D): U.S. Geological Survey Water-Resources Investigations Report 96-4267.”

Langevin, C.D., J.D. Hughes, E.R. Banta, A.M. Provost, R.G. Niswonger, and Sorab Panday. 2018. “MODFLOW 6 Modular Hydrologic Model.” U.S. Geological Survey Software Release. https://doi.org/10.5066/F76Q1VQV.

Langevin, C.D., J.D. Hughes, A.M. Provost, M.J. Russcher, R.G. Niswonger, Sorab Panday, Damian Merrick, and E.R. Banta. 2022. “MODFLOW 6 Modular Hydrologic Model Version 6.2.2: U.S. Geological Survey Software Release, 30 July 2021.” https://doi.org/https://doi.org/10.5066/P97FFF9M.

Langevin, Christian D., Joseph D. Hughes, E.R. Banta, Richard G. Niswonger, Sorab

Panday, and A.M. Provost. 2017. “Documentation for the MODFLOW 6 Groundwater Flow Model.” *U.S. Geological Survey*. https://doi.org/10.3133/tm6A55.

Langevin, Christian D., Alden M. Provost, Sorab Panday, and Joseph D. Hughes. 2022. “Documentation For The MODFLOW 6 Groundwater Transport Model.” *U.S. Geological Survey*, no. Techniques and Methods, book 6, chap. A61: 56. https://doi.org/https://doi.org/10.3133/tm6A61.

Langevin, Christian D., Daniel T. Thorne Jr., Alyssa M. Dausman, Michael C. Sukop, and Weixing Guo. 2008. “SEAWAT Version 4: A Computer Program for Simulation of Multi-Species Solute and Heat Transport.” *U.S. Geological Survey Techniques and Methods Book 6*, no. Techniques and Methods, book 6, chap A22: 39. https://doi.org/10.3133/tm6A22.

Liu, Jiaqi, and Tomochika Tokunaga. 2020. “Regime Identification, Dimensionless Numbers, and Parameter Sensitivity of Variable-Density Flow in Porous Media Based on Numerical Simulations.” *Water Resources Research* 56 (8): 1–19. https://doi.org/10.1029/2020WR027623.

Mancewicz, Lauren K., Alex Mayer, Christian Langevin, and Jason Gulley. 2023. “Improved Method for Simulating Groundwater Inundation Using the MODFLOW 6 Lake Transport Package.” *Groundwater* 61 (3): 421–30. https://doi.org/10.1111/gwat.13254.

Masselink, Gerd, Eddie Beetham, and Paul Kench. 2020. “Coral Reef Islands Can Accrete Vertically in Response to Sea Level Rise.” *Sci. Adv* 6: 3656–66. https://www.science.org.

Masterson, John P, Michael N Fienen, E Robert Thieler, Dean B Gesch, Benjamin T Gutierrez, and Nathaniel G Plant. 2014. “Effects of Sea-Level Rise on Barrier Island Groundwater System Dynamics – Ecohydrological Implications.” *Ecohydrology* 7 (November 2013): 1064–71. https://doi.org/10.1002/eco.1442.

Merritt, Michael L., and Leonard F. Konikow. 2000. “Documentation of a Computer Program to Simulate Lake-Aquifer Interation Using the MODFLOW Ground-Water Flow Model and the MOC3D Solute-Transport Model.” *U.S. Geological Survey Water-Resources Investigations Report 00-4167*.

Mulligan, Ann E., Christian Langevin, and Vincent E.A. Post. 2011. “Tidal Boundary Conditions in SEAWAT.” *Ground Water* 49 (6): 866–79. https://doi.org/10.1111/j.1745-6584.2010.00788.x.

Oberdorfer, June A, Patrick J Hogan, and Robert W Buddemeier. 1990. “Occurrence in a Tidally Dominated System.” *Journal of Hydrology* 120: 327–40.

Post, Vincent E.A., and Georg J. Houben. 2017. “Density-Driven Vertical Transport of

Saltwater through the Freshwater Lens on the Island of Baltrum (Germany) Following the 1962 Storm Flood." *Journal of Hydrology* 551: 689–702. https://doi.org/10.1016/j.jhydrol.2017.02.007.

Ritzi, Robert W., John M. Bukowski, Cindy K. Carney, and Mark R. Boardman. 2001. "Explaining the Thinness of the Fresh Water Lens in the Pleistocene Carbonate Aquifer on Andros Island, Bahamas." *Ground Water* 39 (5): 713–20. https://doi.org/10.1111/j.1745-6584.2001.tb02361.x.

Rotzoll, Kolja, and Charles H. Fletcher. 2013. "Assessment of Groundwater Inundation as a Consequence of Sea-Level Rise." *Nature Climate Change* 3 (5): 477–81. https://doi.org/10.1038/nclimate1725.

Schincariol, Robert A., Franklin W. Schwartz, and Carl A. Mendoza. 1994. "On the Generation of Instabilities in Variable Density Flow." *Water Resources Research* 30 (4): 913–27. https://doi.org/10.1029/93WR02951.

Sheibani, Sorour, Behzad Ataie-Ashtiani, Ammar Safaie, and Craig T. Simmons. 2020. "Influence of Lakebed Sediment Deposit on the Interaction of Hypersaline Lake and Groundwater: A Simplified Case of Lake Urmia, Iran." *Journal of Hydrology* 588 (May). https://doi.org/10.1016/j.jhydrol.2020.125110.

Simmons, Craig T., Kumar A. Narayan, and Robin A. Wooding. 1999. "On a Test Case for Density-Dependent Groundwater Flow and Solute Transport Models: The Salt Lake Problem." *Water Resources Research* 35 (12): 3607–20. https://doi.org/10.1029/1999WR900254.

Sweet, W. V., R. E. Kopp, C. P. Weaver, J. Obeysekera, R. M. Horton, E. R. Thieler, and C. Zervas. 2017. "Global and Regional Sea Level Rise Scenarios for the United States." https://tidesandcurrents.noaa.gov/publications/techrpt83_Global_and_Regional_SLR_Scenarios_for_the_US_final.pdf.

Terry, James P., and Ting Fong May Chui. 2012. "Evaluating the Fate of Freshwater Lenses on Atoll Islands after Eustatic Sea-Level Rise and Cyclone-Driven Inundation: A Modelling Approach." *Global and Planetary Change* 88–89: 76–84. https://doi.org/10.1016/j.gloplacha.2012.03.008.

Vacher, H. L., and T. N. Wallis. 1992. "Comparative Hydrogeology of Fresh-Water Lenses of Bermuda and Great Exuma Island, Bahamas." *Ground Water* 30 (1): 15–20. https://doi.org/10.1111/j.1745-6584.1992.tb00806.x.

Vacher, H L. 1988. "Dupuit-Ghyben-Herzberg Analysis of Strip-Island Lenses." *Geological Societ of America Bulletin*, no. April: 580–92. https://doi.org/10.1130/0016-7606(1988)100<0580:DGHAOS>2.3.CO;2.

Whitaker, F. F., and P. L. Smart. 2000. "Characterising Scale-Dependence of Hydraulic

Conductivity in Carbonates: Evidence from the Bahamas." *Journal of Geochemical Exploration* 69–70: 133–37. https://doi.org/10.1016/S0375-6742(00)00016-9.

Whitaker, Fiona F., and Peter L. Smart. 1997. "Climatic Control of Hydraulic Conductivity of Bahamian Limestones." *Ground Water* 35 (5): 859–68. https://doi.org/10.1111/j.1745-6584.1997.tb00154.x.

Wooding, R. A., Scott W. Tyler, and Ian White. 1997. "Convection in Groundwater below an Evaporating Salt Lake: 1. Onset of Instability." *Water Resources Research* 33 (6): 1199–1217. https://doi.org/10.1029/96WR03533.

Woodroffe, Colin D. 2011. "Subsidence Hypothesis of Reef Development." In *Encyclopedia of Modern Coral Reefs*, 1062–67. Springer, Dordrecht. https://doi.org/10.1007/978-90-481-2639-2_29.

Wu, Xiaojing, Yuansheng Wang, Chengji Shen, and Zhongwei Zhao. 2022. "Variable-Density Flow and Solute Transport in Stratified Salt Marshes." *Frontiers in Marine Science* 8 (January): 1–17. https://doi.org/10.3389/fmars.2021.804526.

Xie, Yueqing, Craig T. Simmons, and Adrian D. Werner. 2011. "Speed of Free Convective Fingering in Porous Media." *Water Resources Research* 47 (11). https://doi.org/10.1029/2011WR010555.

Yu, Xuan, Lu Luo, Peng Hu, Xinjun Tu, Xiaohong Chen, and Junhong Wei. 2022. "Impacts of Sea-Level Rise on Groundwater Inundation and River Floods under Changing Climate." *Journal of Hydrology* 614 (November). https://doi.org/10.1016/j.jhydrol.2022.128554.